Defense Threat Reduction Agency
8725 John J. Kingman Road, MS-6201
Fort Belvoir, VA 22060-6201

DTRA-TR-22-067

TECHNICAL REPORT

A Time-Dependent Physiological Model of Healing Initiated by an Irradiated Superficial Thermal Burn

DISTRIBUTION A. Approved for public release: distribution unlimited.

November 2022

HDTRA1-14-D-0003

Prepared by:
Applied Research Associates, Inc.
801 N. Quincy Street
Suite 700
Arlington, VA 22203

UNIT CONVERSION TABLE

U.S. customary units to and from international units of measurement*

U.S. Customary Units	Multiply by → / ← Divide by†		International Units
Length/Area/Volume			
inch (in)	2.54	$\times 10^{-2}$	meter (m)
foot (ft)	3.048	$\times 10^{-1}$	meter (m)
yard (yd)	9.144	$\times 10^{-1}$	meter (m)
mile (mi, international)	1.609 344	$\times 10^{3}$	meter (m)
mile (nmi, nautical, U.S.)	1.852	$\times 10^{3}$	meter (m)
barn (b)	1	$\times 10^{-28}$	square meter (m^2)
gallon (gal, U.S. liquid)	3.785 412	$\times 10^{-3}$	cubic meter (m^3)
cubic foot (ft^3)	2.831 685	$\times 10^{-2}$	cubic meter (m^3)
Mass/Density			
pound (lb)	4.535 924	$\times 10^{-1}$	kilogram (kg)
atomic mass unit (AMU)	1.660 539	$\times 10^{-27}$	kilogram (kg)
pound-mass per cubic foot ($lb\ ft^{-3}$)	1.601 846	$\times 10^{1}$	kilogram per cubic meter ($kg\ m^{-3}$)
Pound-force (lbf avoirdupois)	4.448 222		Newton (N)
Energy/Work/Power			
electron volt (eV)	1.602 177	$\times 10^{-19}$	joule (J)
erg	1	$\times 10^{-7}$	joule (J)
kiloton (kT) (TNT equivalent)	4.184	$\times 10^{12}$	joule (J)
British thermal unit (Btu) (thermochemical)	1.054 350	$\times 10^{3}$	joule (J)
foot-pound-force (ft lbf)	1.355 818		joule (J)
calorie (cal) (thermochemical)	4.184		joule (J)
Pressure			
atmosphere (atm)	1.013 250	$\times 10^{5}$	pascal (Pa)
pound force per square inch (psi)	6.984 757	$\times 10^{3}$	pascal (Pa)
Temperature			
degree Fahrenheit (°F)	[T(°F) − 32]/1.8		degree Celsius (°C)
degree Fahrenheit (°F)	[T(°F) + 459.67]/1.8		kelvin (K)
Radiation			
activity of radionuclides [curie (Ci)]	3.7	$\times 10^{10}$	per second (s^{-1}‡)
air exposure [roentgen (R)]	2.579 760	$\times 10^{-4}$	coulomb per kilogram ($C\ kg^{-1}$)
absorbed dose (rad)	1	$\times 10^{-2}$	joule per kilogram ($J\ kg^{-1}$§)
equivalent and effective dose (rem)	1	$\times 10^{-2}$	joule per kilogram ($J\ kg^{-1}$**)

*Specific details regarding the implementation of SI units may be viewed at http://www.bipm.org/en/si/.

†Multiply the U.S. customary unit by the factor to get the international unit. Divide the international unit by the factor to get the U.S. customary unit.

‡The special name for the SI unit of the activity of a radionuclide is the becquerel (Bq). ($1\ Bq = 1\ s^{-1}$).

§The special name for the SI unit of absorbed dose is the gray (Gy). ($1\ Gy = 1\ J\ kg^{-1}$).

**The special name for the SI unit of equivalent and effective dose is the sievert (Sv). ($1\ Sv = 1\ J\ kg^{-1}$).

REPORT DOCUMENTATION PAGE

PLEASE DO NOT RETURN YOUR FORM TO THE ABOVE ORGANIZATION.

1. REPORT DATE	2. REPORT TYPE	3. DATES COVERED	
		START DATE	END DATE
11-9-2022	Technical Report		

4. TITLE AND SUBTITLE

A Time-Dependent Physiological Model of Healing Initiated by an Irradiated Superficial Thermal Burn

5a. CONTRACT NUMBER	5b. GRANT NUMBER	5c. PROGRAM ELEMENT NUMBER
HDTRA1-14-D-0003		
5d. PROJECT NUMBER	**5e. TASK NUMBER**	**5f. WORK UNIT NUMBER**

6. AUTHOR(S)

Quintessa Hay, Rachel Jennings, PhD, Angela Reynolds, PhD, Amy Creel,

7. PERFORMING ORGANIZATION NAME(S) AND ADDRESS(ES)

Applied Research Associates, Inc.
801 N. Quincy Street, Suite 700
Arlington, VA 22203

8. PERFORMING ORGANIZATION REPORT NUMBER

9. SPONSORING/MONITORING AGENCY NAME(S) AND ADDRESS(ES)

Defense Threat Reduction Agency - Nuclear Technologies Department, Attn: Dr. Blake
8725 John J. Kingman Road, Mail Stop 6201
Fort Belvoir, VA 22060-6201

10. SPONSOR/MONITOR'S ACRONYM(S)

DTRA-RD-NTS

11. SPONSOR/MONITOR'S REPORT NUMBER(S)

DTRA-TR-22-067

12. DISTRIBUTION/AVAILABILITY STATEMENT

DISTRIBUTION A. Approved for public release: distribution is unlimited.

13. SUPPLEMENTARY NOTES

14. ABSTRACT

Ionizing radiation delays the wound healing process in thermal burns. A model describing the local inflammatory response and early fibroblast activity triggered by a locally irradiated superficial thermal burn is presented. Its features include diminished immune cell infiltration; polarization towards a macrophage phenotype; and fibroblast dysfunction. Numerical simulations show the model's ability to capture the dose-effect relationship between healing time and radiation dose as well as other known biological dynamics.

15. SUBJECT TERMS

Thermal Burn, Radiation, Wound Healing, Inflammation, Modeling, Combined Injury

16. SECURITY CLASSIFICATION OF:			17. LIMITATION OF ABSTRACT	18. NUMBER OF PAGES
a. REPORT	b. ABSTRACT	C. THIS PAGE		
U	U	U	U	43

19a. NAME OF RESPONSIBLE PERSON	19b. PHONE NUMBER *(Include area code)*
Paul K. Blake, PhD, GS-15	571.616.6117

PREVIOUS EDITION IS OBSOLETE.

STANDARD FORM 298 (REV. 5/2020)
Prescribed by ANSI Std. Z39.18

This page intentionally left blank.

Table of Contents

List of Figures

List of Tables

Acknowledgements

We gratefully acknowledge Dr. Paul Blake, Dr. Lawrence Herskowitz, and DTRA's Nuclear Technologies Survivability Division for programmatic support. We would also like to thank MAJ Mostafa Ahmed, MD, MC, USA, Uniformed Services University of Health and Sciences and Dr. Andrea DiCarlo-Cohen, National Institute of Allergy and Infectious Disease for their valuable feedback on the research presented in this technical report. This work was performed under DTRA contract HDTRA1-14-D-0003.

Executive Summary

Ionizing radiation delays the wound healing process in thermal burns, increasing the likelihood of adverse health outcomes, and greater time to return-to-duty. To study the pathophysiological mechanisms unique to such combined injuries, an existing time-dependent physiological model of superficial thermal burns that describes the local inflammatory response and early fibroblast activity was modified to include effects of irradiation. Incorporated immunological features include diminished immune cell infiltration to the wound site due to radiation-induced vascular damage; polarization towards a macrophage phenotype; and fibroblast dysfunction. Further, a differential equation describing the time evolution of pathogen levels in the wound was also added. The model was able to capture experimentally observed delays in wound healing and immune cell infiltration as well as reduced fibroblast proliferation and removal of damage. Additionally, the model exhibited increased pathogen levels and sustained infection with increasing radiation doses. To the authors' best knowledge, this mathematical model of healing initiated by an irradiated thermal burn is the first of its kind, highlighting the complexities presented by combined insults. As the development of this model and others like it continue to evolve, the goal is to build a foundational structure for the construction of physiologically driven models that not only adopt systems-level mechanistic frameworks but also leverage legacy models developed by the Defense Threat Reduction Agency to predict casualty distributions after a nuclear detonation event. Time-dependent models of this nature will allow for dynamic predictions that support all aspects of consequence evaluation in the aftermath of a nuclear detonation to include medical planning, combat power assessment, and other relevant outcomes.

Section 1. Introduction

Developed by Applied Research Associates (ARA) for the Defense Threat Reduction Agency (DTRA), the Health Effects from Nuclear and Radiological Environments (HENRE) engine predicts casualties for given environmental conditions following a nuclear detonation (NUDET) event. In a NUDET event, potential injuries to civilians and military personnel could include air blast related injuries, thermal burns, and ionizing radiation (Reeves 2018). Based on historical evidence, the majority of resulting casualties are expected to be caused by more than one insult, especially radiation exposure combined with thermal injury (Iijima 1982; Kishi 2000; Pellmar and Ledney 2005; DiCarlo et al. 2008; Palmer et al. 2011). Other combined insults could include radiation exposure with concomitant puncture wounds, overpressure injuries, hemorrhage, fracture, and infections.

Combined insults are associated with greater tissue damage, and increased risk of adverse outcomes such as lethality (Alpen et al. 1954), secondary infection (Kiang et al. 2010b), and sepsis (Ledney et al. 1991; Yan et al. 1995). Moreover, synergistic effects have also been observed (Brooks et al. 1952; Alpen et al. 1954), adding further complexity to an already challenging problem. Understanding the collective effects of combined injury, including the complex pathophysiology, is fundamental for gauging injury severity and outcome. Thus, current research efforts are focused on developing time-dependent physiological models (TDPMs) of injuries resulting from combined insults starting with irradiated thermal burns.

Since ionizing radiation delays the healing process (Stromberg et al. 1967; Zelman et al. 1968; Zawaski et al. 2014), wound healing presents a path towards this goal. A TDPM of human immune response following superficial thermal burns was previously formulated by ARA (Jennings et al. 2022a). This model aimed to capture hematopoietic and immunologic events across the bone marrow, lymphatic tissues, blood vessels, and local wound site. As superficial thermal injuries do not disrupt hematopoietic homeostasis, the model was reduced to a subsystem of eight ordinary differential equations reflecting the innate and adaptive immune dynamics (inflammation phase) as well as early fibroblast activity (proliferation phase) at the injury site. This reduced model captured longer healing times associated with more severe burn injury as well as other critical dynamics, such as sustained inflammation due to blocked removal of debris. This technical report expands the reduced TDPM for superficial thermal burns to include effects of ionizing radiation exposure.

While irradiation delays wound healing, the pathophysiological responses that lead to such an effect depend on the extent of the exposure: whole-body, partial-body or local. Whole-body radiation involves the hematopoietic system (Yan et al. 1995; Cheng et al. 2002; Ran et al. 2003), yet there is considerably less impact near and in the wound site (Vegesna et al. 1993). Circulating immune cells that form a “resource pool” are depleted following whole-body ionizing radiation, delaying the onset and reducing the magnitude of the inflammatory response at the site of injury (Vegesna et al. 1993). However, there is evidence to suggest that this kind of irradiation can damage dermal fibroblasts (Qu et al. 2004), which could play a key role in the delaying the healing process. In contrast, local ionizing radiation damages not only critical repair cells, specifically fibroblasts, but also the vasculature (Vegesna et al. 1993), suggesting why infiltration to the wound by inflammatory cells is reduced (Sweeney et al. 1997; Iddins et al. 2022). Ionizing radiation has the capacity to injure a considerable number of tissues in the body, presenting a formidable challenge for capturing its effects in a mathematical model. Consequently, to advance the

development of mechanistic, time-dependent mathematical models of combined injury (herein including only thermal and ionizing radiation) in a well-posed and systematic manner, modifications for whole-body ionizing radiation must be delineated from those for localized exposures. Moreover, with dermal fibroblasts being damaged regardless of the fraction of the body exposure, it is critical that the mathematical representation capturing this process in the model be well-understood.

Currently, existing radiation HENRE models assume a whole-body exposure event. However, localized irradiated superficial thermal burns are a critical priority for the military. Soldiers have varying degrees of skin protection from natural and man-made structures, e.g., armored vehicles, foxholes, and buildings, which can reduce not only the radiation dose, but also the extent of the exposure (Reeves 2018). Thus, localized exposures serve as a starting point for capturing the effects of combined insults in the non-idealized setting. Moreover, acute clinical manifestations of localized irradiation of the skin can include erythema, dry and moist desquamation, and amplified cytokine production with a dose dependent relationship (Ryan 2012). These effects are correlated with performance decrement, demonstrating alignment with HENRE's current priorities. Consequently, to advance the development of a mechanistic TDPM of combined injury in a well-posed and systematic manner, localized irradiation is only considered in the present model.

This technical report begins by presenting a TDPM that considers the immune response at the site of injury, including populations of neutrophils, macrophages, lymphocytes, and fibroblasts as well as equations for damage and debris and a newly introduced pathogen population. As this model represents an extension of a previous one for superficial thermal burn alone, necessary adjustments to account for the effects of localized irradiation were made. New model processes will be discussed, such as infection by pathogens at the burn site. Numerical simulations are then presented to demonstrate the ability of the TDPM to reproduce known biological trends.

Section 2. Effects of Ionizing Radiation

Cellular damage caused by ionizing radiation is typically due to direct or indirect damage of the DNA strands (Hall and Giaccia 2012). As a result, cells are more likely to be damaged during specific phases of cellular replication. Consequently, highly proliferative cells are more likely to suffer deleterious effects from ionizing radiation (Ryan 2012). Additionally, cells in different phases of mitosis or those that do not divide frequently may be minimally affected. The skin, in general, is considered a highly radiosensitive organ, but individual skin cells have varying degrees of radiosensitivity. Fibroblasts and lymphocytes, for instance, are considered highly radiosensitive (Geara et al. 1992) while others, such as differentiated macrophages, are more radioresistant (Heylmann et al. 2021). Some subpopulations of lymphocytes like regulatory T cells are also considered to be relatively radioresistant (Beauford et al. 2020) but the intricacies of subpopulation-based radiosensitivies are not considered in the present model.

The fraction of the body exposed to ionizing radiation, namely whole-body, partial-body, or localized, can vary based on the nature of the exposure (Vegesna et al. 1993; DiCarlo et al. 2011). The effects of whole body radiation are complex, involving numerous tissues including the hematopoietic system, gastrointestinal tract, cardiovascular system, skin, kidneys, and other radiosensitive organs (United Nations Scientific Committee on the Effects of Atomic Radiation 1982). There is also evidence to suggest that it can damage dermal fibroblasts (Qu et al. 2004). Local irradiation, on the other hand, is generally confined to a smaller area (Vegesna et al. 1993; Iddins et al. 2022). Consequently, cells in the hematopoietic system and lymphatic tissues, as well as circulating cells, are not normally significantly affected by local radiation exposures. Combining localized radiation with a thermal burn injury will thus yield a model confined to a specific area of the body.

Superficial thermal burns affect only the epidermis and papillary dermis of the skin (Evers et al. 2010; Reeves 2018; Abazari et al. 2020; Jeschke et al. 2020). For prompt localized exposures, the impact of ionizing radiation will likely extend slightly beyond the boundary of the thermal burn injury; that is, the effects of ionizing radiation are concentrated in the immediate tissue surrounding the thermal burn. Thus, for an irradiated thermal burn, we consider cells within the burn injury boundary to be destroyed by thermal radiation, whereas those in the adjacent tissue can be damaged by ionizing radiation.

Not all cells of interest have resident populations in the surrounding tissue. Neutrophils, for example, are not abundant in healthy skin (Nguyen and Soulika 2019), and thus will not be damaged by irradiation. On the other hand, macrophages, T lymphocytes, and fibroblasts do have normally quiescent resident populations in the healthy tissues, and thus may be impacted by acute radiation exposure. However, damage to these tissue-resident cells depends on the extent of radiation injury, the dose received, and the radiosensitivity of the cell itself.

Section 3. TDPM of Thermal Burn and Ionizing Radiation

3.1 TDPM Compartments and Variables

Since localized exposures do not normally impact tissues outside of the wound (Vegesna et al. 1993), cellular dynamics in the bone marrow, lymphatic tissues, and blood vessels remain at steady state; that is, the quasi-steady state assumption still applies to the systemic compartments. Thus, the model need only consider dynamics in and near the boundary of the wound site with the influx rates from the hematopoietic and lymphatic systems assumed to be constant.

The TDPM for an irradiated superficial thermal burn consists of 15 ordinary differential equations (ODEs). Figure 1 provides a schematic of the state variables and their relationships across two compartments: the wound itself and the immediate surrounding tissue. State variables are represented using circles and squares. The solid black lines indicate transitions between different cellular states. Solid lines that feedback into the state variable itself indicate proliferation. Initiated cellular interactions are captured by dotted lines and remain locally concentrated. Blue and white colors are used to distinguish between up-regulatory (i.e., increasing in response to the cells themselves) and destructive/inhibitory relationships, respectively. The toxic triangles indicate cell transitions and interactions affected by ionizing radiation that have been incorporated into the model.

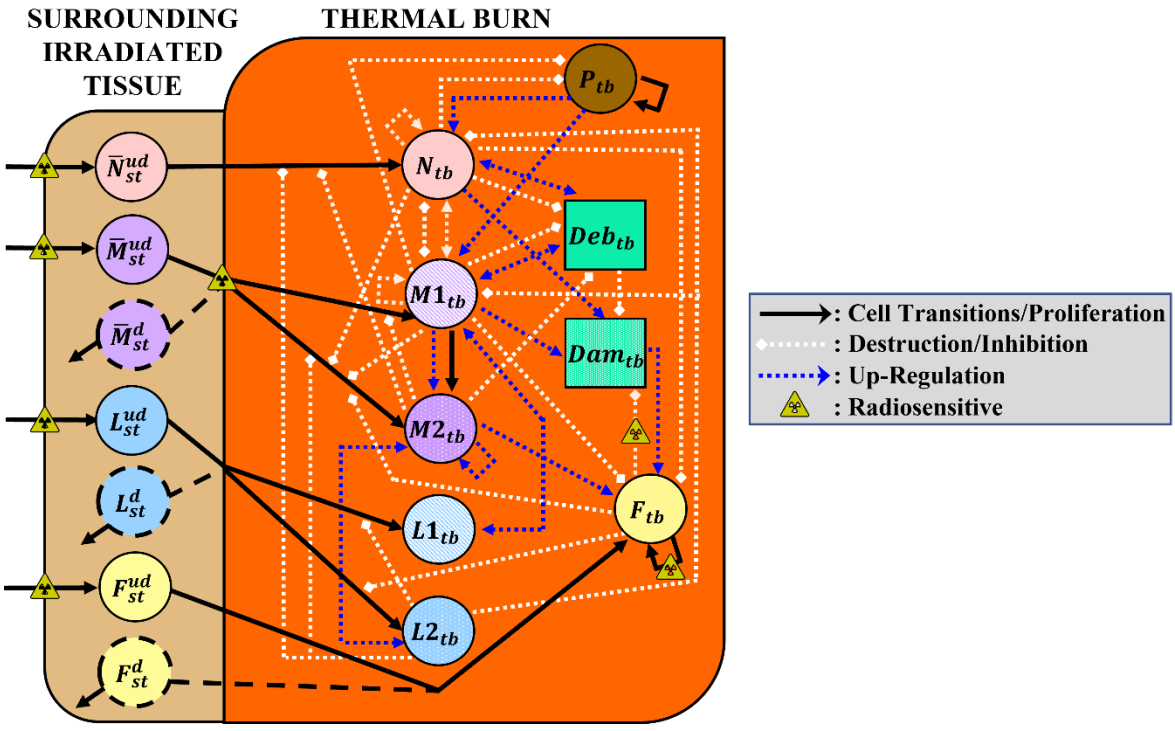

Figure 1. Schematic diagram of irradiated superficial thermal burn, the state variables, and their relationships.

Table 1 lists the symbols and corresponding descriptions of the state (or dynamic) variables[1] included in the TPDM. State variables are assumed to represent the cell types and their signaling molecules.

Table 1. TDPM State Variable Symbols and Definitions by Compartment.

SYMBOL	DESCRIPTION
t	Time (in hours)
$Dose_{rad}$	Radiation absorbed dose (in Gy)
Blood Vessels	
$\bar{N}_{bv}$	Resting neutrophils in circulation*
$\overline{M}_{bv}$	Resting monocytes in circulation*
L_{bv}	Newly activated T lymphocytes migrating to the site(s) of injury via the blood vessels*
Local Irradiated Tissue	
$\bar{N}_{st}^{ud}$	Resting neutrophils in the surrounding tissue
$\bar{M}_{st}^{ud}$	Undamaged, resting, tissue-resident monocytes/macrophages in the surrounding tissue
$\bar{M}_{st}^{d}$	Damaged, resting, resident monocytes/macrophages in the surrounding tissue
F_{ct}	Resident (proliferative) fibroblasts in the connective tissue*
F_{st}^{ud}	Undamaged, resident fibroblasts in the surrounding tissue
F_{st}^{d}	Damaged resident fibroblasts in the surrounding tissue
L_{st}^{ud}	Undamaged resident lymphocytes in the surrounding tissue
L_{st}^{d}	Damaged resident T lymphocytes in the surrounding tissue
Local Thermal Burn	
Dam_{tb}	Damaged tissue (unitless)
Deb_{tb}	Debris (unitless)
N_{tb}	Activated neutrophils at the wound site
$M1_{tb}$	Classically activated macrophages (M1) at the wound site
$M2_{tb}$	Alternatively activated macrophages (M2) at the wound site
F_{tb}	Fibroblasts at the wound site
$L1_{tb}$	Pro-inflammatory T lymphocytes, including $\gamma\delta$-T cells, TH1 cells, and TH17 cells, at the wound site
$L2_{tb}$	Anti-inflammatory T lymphocytes, including TH2 cells and regulatory T cells, at the wound site
P_{tb}	Pathogen levels at the wound site
*State variables that are assumed to be at steady state prior to and following irradiated thermal injury.	

An ODE was constructed for each state variables based on known physiological behaviors and interactions supported by peer-reviewed literature. Let N, M, L, and F denote granulocyte/neutrophil, monocyte/macrophage, T lymphocyte, and fibroblast populations,

[1] State (or dynamic) variables refer to those quantities whose temporal evolution will eventually be described by a system of ODEs, reflecting that their levels change with time.

respectively, with subscripts (st and tb) indicating the compartment. Cells damaged by ionizing radiation at the thermal burn site are also not accounted for, since all cells within the burn injury boundary are assumed to be destroyed by thermal radiation. On the other hand, only resident cell populations in the surrounding tissue can be either damaged or undamaged, depending on the extent of radiation injury, the dose received, and the radiosensitivity of the cell.

The model assumes radiation causes cells to enter a damaged state before they undergo an early cell death, and this effect is instantaneous at the time of exposure. Thus, damaged cells are modeled in the surrounding tissue with equations that decay over time. Moreover, the model assumes that damaged proliferating cells cannot reproduce, as this is often the most clinically relevant phenomenon of cellular radiation damage (Joiner 2018) and other mathematical models have used this assumption (Hanin and Zaider 2013). Superscripts d and ud are used to distinguish between the damaged and undamaged cells, respectively. This approach aligns with existing hematopoietic models in HENRE created for DTRA (Wentz et al. 2015), and other mathematical models and reviews (Gu et al. 2002; Hanin and Zaider 2013).

Variables in the surrounding tissue then migrate into the local wound compartment representing the thermal burn. Radiation-induced cellular damage is concentrated to resident cell populations only, such as macrophages, T lymphocytes, and fibroblasts in the local surrounding tissue. Recall that neutrophils do not naturally reside in tissue in the absence of injury. However, they are tracked in the surrounding tissue compartment to represent undamaged neutrophils migrating from the blood vessels to the thermal burn site.

3.2 Initial Conditions: Radiation-Induced Cell Damage

For the purposes of this model, we consider only a prompt radiation exposure at the initial time of injury, as this is most consistent with a NUDET event within the radius of thermal injury (Brooks et al. 1952). Macrophages, T lymphocytes, and fibroblasts are the only tissue-resident cell populations in the model. Thus, their corresponding initial values are non-zero, whereas neutrophils in the surrounding tissue will be zero. As mentioned previously, the radiosensitivities of the cells vary and thus, the initial conditions for the damaged cells will vary. The overall effects of ionizing radiation are also dependent on the dose and type of radiation (United Nations Scientific Committee on the Effects of Atomic Radiation 2006) thus, these variations must also be considered.

Initial populations of damaged cells will be calculated using a survival probability curve. Past models of the hematopoietic system have used single-target, single-hit inactivation and multi-target, single-hit inactivation (Smirnova 2012; Wentz et al. 2015). These model cell survival as a function of radiation dose, $Dose_{rad}$, and a critical dose value $Dose_{crit}$, the dose that gives an average of one hit per target (Joiner 2018). Both models produce relatively accurate estimates of survival, but lack in some specific details, particularly when dealing with cell survival at low doses. The single-target, single-hit inactivation is a relatively simple exponential model based on Poisson statistics and is most relevant to viral and bacterial populations, due to the simple mechanics involved in radiation damage for these organisms (Joiner 2018). The multi-target, single-hit inactivation is more typically applicable to mammalian cells where a "shouldered" survival curve is considered more accurate (Goodhead 1985). This model assumes cells have n sensitive regions in their DNA strands and thus require more targets to be hit before cellular death is induced. This assumption, however, creates an almost horizontal survival curve for low doses that is not supported by the research, so two component models were considered to combat this effect (Joiner

2018). These models are often considered too complicated for the process being modeled and are not often used.

Another popular method for predicting the proportion of surviving cells for a given radiation dose is the linear-quadratic (LQ) model (Chadwick and Leenhouts 1973). This model is widely used in both experimental and clinical settings of radiobiology, and it can be applied to both *in vitro* and *in vivo* models (Brenner 2008; Kuang et al. 2016). If $p_{survival}$ denotes the probability of cell survival and $Dose_{rad}$ is radiation dose, then the LQ model satisfies

$$p_{survival} = \exp(-a \cdot Dose_{rad} - b \cdot Dose_{rad}^2) \quad (1)$$

where a (in Gy^{-1}) and b (in Gy^{-2}) are unknown parameters describing the contribution of non-repairable and repairable cellular damage, respectively. The values for a and b can differ significantly between cell types and individuals.

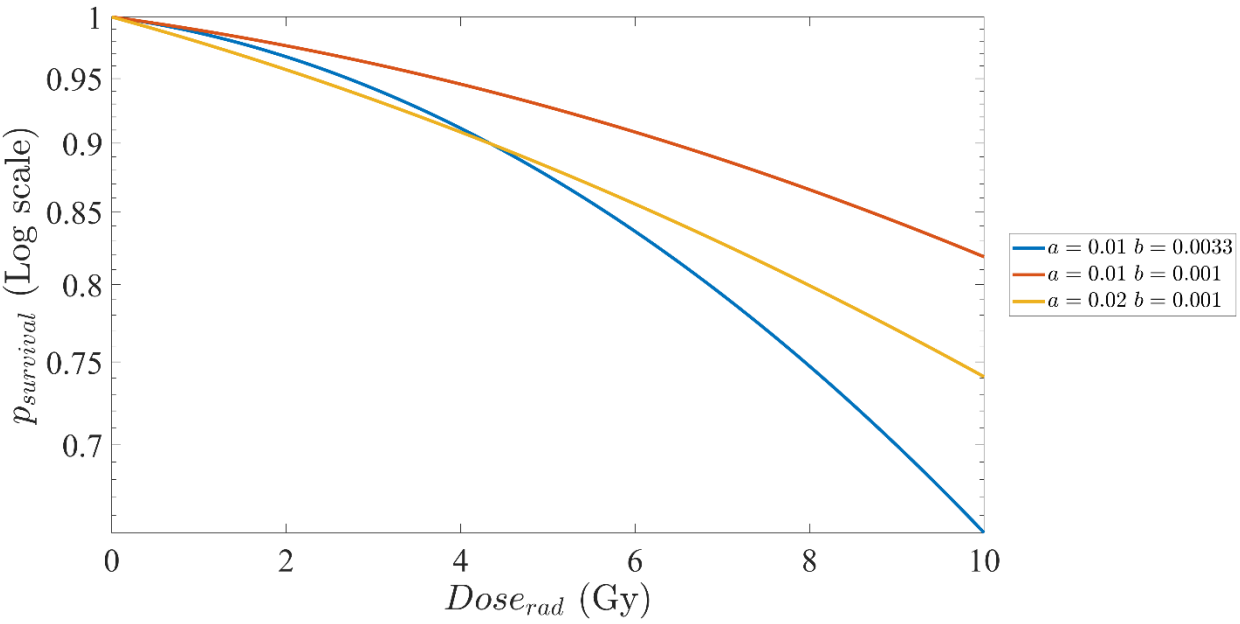

Figure 2. Cell survival curve of the linear-quadratic model.

Figure 2 plots $p_{survival}$ versus $Dose_{rad}$ as determined by Eqn. (1) for three different combinations of a and b. The concave-down shape is generally similar to that of other models mentioned before but provides a better description for cell survival in the lower dose regions (0-3 Gy) (Joiner 2018). The fraction a/b is often used to characterize the radiosensitivity of a particular cell (or tissue) type, providing a measure of the curvature in the survival curve and thus, a classification scheme. The fraction for the combinations of a and b from Figure 2 are 3.03 Gy (blue), 10 Gy (red), and 20 Gy (yellow). A ratio close to 3 indicates pronounced curvature with high killing rates as the dose increases, whereas 10 suggests a near constant killing rate (McMahon 2019), which can be seen from the approximately linear behavior of the yellow curve in Figure 2. Thus, 3 and 10 are commonly regarded as being characteristic of a generic cell and those found in highly proliferative tissues such as the skin. Note that values for this fraction have not been demonstrated to fall below one (Lewin et al. 2018).

The "unified repair model", which allows for the possibility that cellular damage can be repaired (Curtis 1986), provides a different approach for computing $p_{survival}$. However, as this model produces almost identical cell survival curves to those of the LQ model, save for doses associated with very small survival levels, the LQ model remains the preferred method. It is worth mentioning that the LQ framework has also been adopted by the International Commission on Radiological Protection for use in radiological models (Clarke et al. 1991). Thus, here we use the LQ model to calculate the initial populations of damaged cells where the ratio of undamaged cells to damaged cells is equivalent to the probability of survival calculated in Eqn. (1).

Table 2 summarizes the initial conditions assigned to each state variable illustrating how the LQ model given by Eqn. (1) is incorporated into those values for tissue-resident state variables.

Table 2. Radiation-independent and -dependent initial conditions for the TDPM.

VARIABLE	INITIAL CONDITION
Local Irradiated Tissue	
$\bar{N}_{st}^{ud}(0)$	0
$\bar{M}_{st}^{ud}(0)$	$\bar{M}_{st,0}\, e^{-a_m Dose_{rad} - b_m Dose_{rad}^2}$
$\bar{M}_{st}^{d}(0)$	$\bar{M}_{st,0}(1 - e^{-a_m Dose_{rad} - b_m Dose_{rad}^2})$
$F_{st}^{ud}(0)$	$F_{st,0}\, e^{-a_f Dose_{rad} - b_f Dose_{rad}^2}$
$F_{st}^{d}(0)$	$F_{st,0}\, (1 - e^{-a_f Dose_{rad} - b_f Dose_{rad}^2})$
$L_{st}^{ud}(0)$	$L_{st,0}\, e^{-a_l Dose_{rad} - b_l Dose_{rad}^2})$
$L_{st}^{d}(0)$	$L_{st,0}\, (1 - e^{-a_l Dose_{rad} - b_l Dose_{rad}^2})$
Local Thermal Burn	
$Dam_{tb}(0)$	0.9*
$Deb_{tb}(0)$	$Dam_{tb}(0)$
$N_{tb}(0)$	0
$M1_{tb}(0)$	0
$M2_{tb}(0)$	0
$F_{tb}(0)$	0
$L1_{tb}(0)$	0
$L2_{tb}(0)$	0
$P_{tb}(0)$	0.8**

Notes: $\bar{M}_{st,0}$, $L_{st,0}$, and $F_{st,0}$ are strictly positive constants such that each is less than or equal to its corresponding healed steady-state value, i.e.,

$$0 < \bar{M}_{st,0} \leq \frac{s_{mr}}{d_{mr}}, \quad 0 < L_{st,0} \leq \frac{s_{lr}}{d_{lr}}, \quad 0 < F_{st,0} \leq \frac{s_f}{d_{fr} - k_{ftb}^{ud}}.$$

The selected values for $\bar{M}_{st,0}$, $L_{st,0}$, and $F_{st,0}$ are provided in Appendix A.

* The value of 0.9 for $Dam_{tb}(0)$ and $Deb_{tb}(0)$ represents a minor superficial, partial-thickness burn with support for it demonstrated elsewhere (Jennings et al. 2022a, 2022b).

** $P_{tb}(0) = 0.8$ lies within the range of values employed by other mathematical models (Reynolds et al. 2006; Menke et al. 2010; Segal et al. 2012; Cooper et al. 2015)

3.3 Model Equations

The TDPM aims to study the inflammatory and early fibroblast activity of wound healing initiated by an irradiated thermal burn. The model builds upon an existing formulation for superficial thermal injury (Jennings et al. 2022a), but dynamics involving cells in the surrounding tissue, in particular, needed to be derived. As a result, in the following subsections, we highlight only the new variables and expressions distinct from the foundational model, which represent effects due to irradiation (i.e., delayed infiltration of immune cells to the burn site; polarization of activated macrophage phenotypes; impaired fibroblast proliferation and collagen deposition; pathogen contamination at the burn site; and phagocytic immune cell activation by pathogens). Model processes not discussed are assumed to be unaffected by radiation. This includes phagocytosis of debris by neutrophils and macrophages and the inhibition of regulatory T cells to limit collateral damage caused by neutrophils (N_{tb}) and M1 macrophages ($M1_{tb}$).

The ODEs forming the model (Eqns. (5)-(32)) utilize the auxiliary functions defined below.

$$\Omega_i(X; Y_1, Y_1^\infty, \dots, Y_m, Y_m^\infty) = \frac{X}{1 + \left(\frac{Y_1}{Y_1^\infty}\right)^2 + \dots + \left(\frac{Y_m}{Y_m^\infty}\right)^2} \tag{2}$$

$$\Omega_H(X, n, X_H) = \frac{X^n}{X_H^n + X^n} \tag{3}$$

$$v(t, Dose_{rad}; \gamma) = \begin{cases} 1, & Dose_{rad} = 0 \\ 1 - exp\left(-\frac{\gamma}{Dose_{rad}} t\right), & Dose_{rad} > 0 \end{cases} \tag{4}$$

Note that the mathematical representation for the inhibition function, $\Omega_i(\cdot)$ is commonly adopted in the literature (Chow et al. 2005; Reynolds et al. 2006; Menke et al. 2010; Segal et al. 2012; Cooper et al. 2015; Day et al. 2015; Torres et al. 2019; Minucci et al. 2021) .

3.3.1. Damage and Debris

The equations for damage and debris (Eqns. (5) and (6), respectively) follow the formulation in the thermal burn model, reflecting an assumption that damage and debris result from thermal injury and not radiation (details are given in (Jennings et al. 2022a)).

$$\begin{aligned} \frac{dDam_{tb}}{dt} = {} & k_{dn}\Omega_H(\Omega_i(N_{tb}; L2_{tb}, L2_2^\infty), 6, N_H) \\ & + k_{dm1}\Omega_H(\Omega_i(M1_{tb}; L2_{tb}, L2_2^\infty), 6, M1_H) \\ & - \rho_{dam}\Omega_i(Dam_{tb}; Deb_{tb}, Deb_{dam}^\infty) \\ & - \Omega_i\left(F_{tb}; F_{st}^d, \omega_{dam}\right)k_{df}\Omega_i(Dam_{tb}; Deb_{tb}, Deb_{dam}^\infty) \end{aligned} \tag{5}$$

$$\begin{aligned}\frac{dDeb_{tb}}{dt} = {} & k_{dn}\Omega_H(\Omega_i(N_{tb}; L2_{tb}, L2_2^{\infty}), 6, N_H) \\ & + k_{dm1}\Omega_H(\Omega_i(M1_{tb}; L2_{tb}, L2_2^{\infty}), 6, M1_H) \\ & - k_{dnp}N_{tb}\Omega_H(Deb_{tb}, 1, Deb_H) \\ & - k_{dm1p}\Omega_i(M1_{tb}; N_{tb}, N_1^{\infty})\Omega_H(Deb_{tb}, 1, Deb_H) \\ & - k_{dm2p}\Omega_i(M2_{tb}; N_{tb}, N_1^{\infty})\Omega_H(Deb_{tb}, 1, Deb_H) - d_{deb}Deb_{tb}\end{aligned} \tag{6}$$

The only change made is the inclusion of an inhibitory multiplier, $\Omega_i\left(F_{tb}; F_{st}^d, \omega_1\right)$, on the last term of Eqn. (5). Early repair processes captured by collagen deposition from fibroblasts is modeled in the last term of Eqn. (5). Collagen has been observed to be a good marker of tissue damage resolution in other mathematical models of wound healing (Segal et al. 2012). While not explicitly represented in the present model, the accumulation of collagen is indirectly captured by the decrease in the Dam_{tb} variable.

Radiation has been observed to inhibit deposition of collagen by fibroblasts (Vegesna et al. 1993; Dormand et al. 2005; Liu et al. 2005). Collagen produced by fibroblasts is not only of a lower quality, but also its deposition in the extracellular matrix of tissues is irregular. The main observation is decreased collagen deposition compared to non-irradiated wounds, but can also include overproduction of low-quality collagen resulting in fibrosis (Dormand et al. 2005). However, fibrosis occurs on a large time scale (years) (Bentzen et al. 1989), and is thus not of interest in the current model. Reduced collagen deposition will, impair early tissue repair and delay or prevent proper healing included in this model. It's impairment has also been show to follow a dose-dependent relationship (Chen et al. 2019). Again, we employ an inhibitory function $\Omega_i\left(F_{tb}; F_{st}^d, \omega_{dam}\right)$ that is both time- and dose-dependent to the last term of Eqn. (5) modeling removal of damage by collagen deposition from fibroblasts. Impaired removal of damage in the wound will result in persistent inflammation and the inability to resolve the wound.

3.3.2. Neutrophils

The ODE for activated neutrophils at the local wound site (N_{tb}) remains similar to that in the previous thermal burn model despite a slight difference in variable nomenclature as well as the addition of a compartment in the surrounding tissue. The neutrophil equations are provided below.

$$\frac{d\bar{N}_{st}^{ud}}{dt} = v(t, Dose_{rad}; \gamma_n)s_{nr} - R_n\bar{N}_{st}^{ud} - d_{nr}\bar{N}_{st}^{ud} \tag{7}$$

$$\begin{aligned}\frac{dN_{tb}}{dt} = {} & R_n\bar{N}_{st}^{ud} - k_{nm1p}N_{tb}\Omega_i(M1_{tb}; N_{tb}, N_1^{\infty}) - k_{nm2p}N_{tb}\Omega_i(M2_{tb}; N_{tb}, N_1^{\infty}) \\ & - d_nN_{tb}\end{aligned} \tag{8}$$

where

$$R_n = \Omega_i\left(k_{nd}Deb_{tb} + k_{np}P_{tb} + k_{nn}N_{tb}; M2_{tb}, M2^{\infty}, L2_{tb}, L2_1^{\infty}\right) \tag{9}$$

$$s_{nr} = \bar{\eta}_{bvtb}\bar{N}_{bv}. \tag{10}$$

The derivation of the first term is only changed by the fact that influx from the blood vessels feeds into the population in the surrounding tissue rather than directly into the thermal burn

compartment. The influx from the blood vessels, s_{nr}, also includes an inhibitory multiplier $v(\cdot)$. Localized ionizing radiation damages the vasculature surrounding the burn wound (Vegesna et al. 1993; Iddins et al. 2022), resulting in delayed infiltration of recruited neutrophils, monocytes, T lymphocytes, and fibroblasts into the wound (Sweeney et al. 1997). To capture this effect in the model, an exponentially decaying inhibitory function, as defined in Eqn. (4), is multiplied by the influx terms from the blood vessels for neutrophils, monocytes, and T lymphocytes and the influx term from the connective tissue for the fibroblasts. This functional form allows for inhibition that is both time- and dose-dependent as illustrated in Figure 3. The current functional form for inhibition assumes immune cell infiltration will be restored to its non-irradiated levels (i.e., burn only). If immune cell infiltration remains impaired for all of time due to permanent vasculature damage, this term could be adapted in future models.

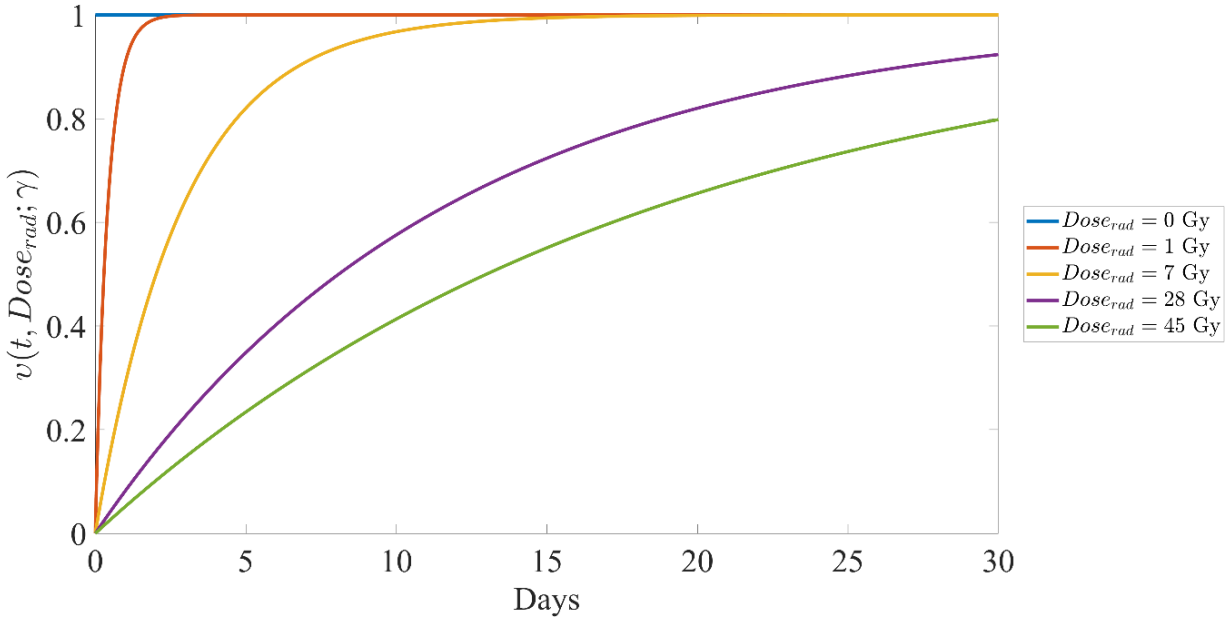

Figure 3. Plot of the decaying inhibitory function defined by Eqn. (4) with $\boldsymbol{\gamma = 0.1}$ for increasing prompt radiation doses.

3.3.3. Monocytes and Macrophages

The derivation of the macrophage equations requires a bit more attention since undamaged and damaged monocytes will contribute to the activated populations in the burn region. The undamaged cell types have a very similar equation to the resting monocytes/macrophages (Jennings et al. 2022a). Recall that superscript *d* denotes an instantaneous radiation-induced damage state that triggers an early cell death. However, damaged monocytes ($\bar{M}_{st}^{d}$) lack a source term and simply decay through activation toward M1 or M2 phenotypes, or by standard decay. While macrophages are considered to be damaged by irradiation, they are relatively radioresistant compared to other immune cells (Heylmann et al. 2021).

Moreover, studies have shown macrophage phagocytic capabilities and chemotaxis are preserved following irradiation (Pinto et al. 2016). Thus, the model assumes that differentiation of damaged tissue monocytes/macrophages into M1 and M2 phenotypes within the burn remains unaffected and contributes to functioning populations denoted as $M1_{tb}$ and $M2_{tb}$, respectively. The monocyte/macrophage populations in the thermal burn then have an influx rate of R_{m1} or R_{m2}

from both the undamaged and damaged populations in the surrounding tissue. Additionally, an inhibitory function (described in the previous section) is multiplied by the source term (s_{mr}) to reflect radiation damage to the surrounding vasculature. The rate of differentiation to M2 (R_{m2}) is also inhibited by radiation. The equations for monocytes/macrophages in the surrounding tissue and macrophages in the thermal burn are given below.

$$\frac{d\bar{M}_{st}^{ud}}{dt} = v(t, Dose_{rad}; \gamma_m)s_{mr} - R_{m1}\bar{M}_{st}^{ud} - \Omega_i\left(R_{m2}; \bar{M}_{st}^{d}, \omega_{m2}\right)\bar{M}_{st}^{ud} - d_{mr}^{ud}\bar{M}_{st}^{ud} \tag{11}$$

$$\frac{d\bar{M}_{st}^{d}}{dt} = -R_{m1}\bar{M}_{st}^{d} - \Omega_i\left(R_{m2}; \bar{M}_{st}^{d}, \omega_{m2}\right)\bar{M}_{st}^{d} - d_{mr}^{d}\bar{M}_{st}^{d} \tag{12}$$

$$\frac{dM1_{tb}}{dt} = R_{m1}\left(\bar{M}_{st}^{ud} + \bar{M}_{st}^{d}\right) - \theta_{m1m2}\left[k_{nm1p}N_{tb}\Omega_i(M1_{tb}; N_{tb}, N_1^{\infty})\right] - d_{m1}M1_{tb} \tag{13}$$

$$\frac{dM2_{tb}}{dt} = \Omega_i\left(R_{m2}; \bar{M}_{st}^{d}, \omega_{m2}\right)\left(\bar{M}_{st}^{ud} + \bar{M}_{st}^{d}\right) + \theta_{m1m2}\left[k_{nm1p}N_{tb}\Omega_i(M1_{tb}; N_{tb}, N_1^{\infty})\right] - d_{m2}M2_{tb} \tag{14}$$

where

$$R_{m1} = \Omega_i\left(k_{m1d}Deb_{tb} + k_{m1p}P_{tb} + k_{m1n}N_{tb} + k_{m1m1}M1_{tb} + k_{m1l1}L1_{tb}; M2_{tb}, M2^{\infty}, L2_{tb}, L2_1^{\infty}\right) \tag{15}$$

$$R_{m2} = \Omega_i(k_{m2m1}M1_{tb} + k_{m2m2}M2 + k_{m2l2}L2; N_{tb}, N_1^{\infty}, M1_{tb}, M1_1^{\infty}, F_{tb}, F^{\infty}) \tag{16}$$

$$s_{mr} = \overline{\mu}_{bvtb}\overline{M}_{bv} \tag{17}$$

Ionizing radiation polarizes macrophages towards either the pro-inflammatory (M1) or anti-inflammatory (M2) phenotype depending on the dose (Rödel et al. 2012). At low doses (maximum of 12 Gy at less than 1.0 Gy/fraction), radiation induces the anti-inflammatory phenotype, whereas higher doses (prompt doses above 2 Gy or fractionated above 40 Gy) favor the pro-inflammatory (Rödel et al. 2015). Radiation-induced polarization of the macrophage phenotype is an emerging and highly active area of research for a range of conditions, not just radiation combined injury (Shi and Shiao 2018; Deloch et al. 2019; Chen et al. 2022; Jo et al. 2022). Proper resolution of inflammation involves a delicate balance of a pro- and anti-inflammatory response, thus perturbations in macrophage polarization can cause unfavorable effects. Pro-inflammatory immunological cells provide the primary protection against foreign bacteria and are necessary for removal of damaged or diseased cells. However, over-expression of pro-inflammatory cells and mediators can induce tissue damage and prevent resolution of inflammation (Duffield 2003). Increased activation towards anti-inflammatory phenotypes can also result in long term health risks. When discussing the balance of the pro- and anti-inflammatory cells in the context of wound healing, we are often most interested in chronic inflammation marked by an uncontrollable pro-inflammatory response, since the effects are observed early in the healing process and prevent progression towards healing (Diegelmann and Evans 2004). The anti-inflammatory phenotype of macrophages, in particular, is essential in signaling tissue repair (Mosser and Edwards 2008) and thus an unbridled pro-inflammatory response will result in a chronic, non-healing wound.

Current research involving radiation-induced macrophage polarization has not described the exact mechanisms by which this switch in activation occurs. Given the prolific evidence of increased pro-inflammatory cytokines following irradiation (Schäffer et al. 2002; Kiang et al. 2010a; DiCarlo et al. 2020), it is natural to assume that this overexpression of pro-inflammatory cytokines could be the mechanism by which activation towards the M1 phenotype occurs. Our current model considers the model variables to be populations of the cell as well as their corresponding cytokines and other mediators. Thus, many processes typically regulated by cytokines and other mediators are instead dependent on the associated variable. For this reason, the altered macrophage activation is dependent on the amount of damaged macrophage cells ($\overline{M}_{st}^{d}$). This allows for both time- and dose-dependent inhibition of the activation process toward the M1 phenotype. This can be observed in Figure 4. The left shows the scaled $M1_{tb}$ ratio to total macrophages in the thermal burn while the right displays the corresponding Dam_{tb} value over time. The plots exhibit the increased and prolonged activation toward the M1 phenotype with increasing $Dose_{rad}$ as well as delayed wound healing exhibited by delayed removal of Dam_{tb}.

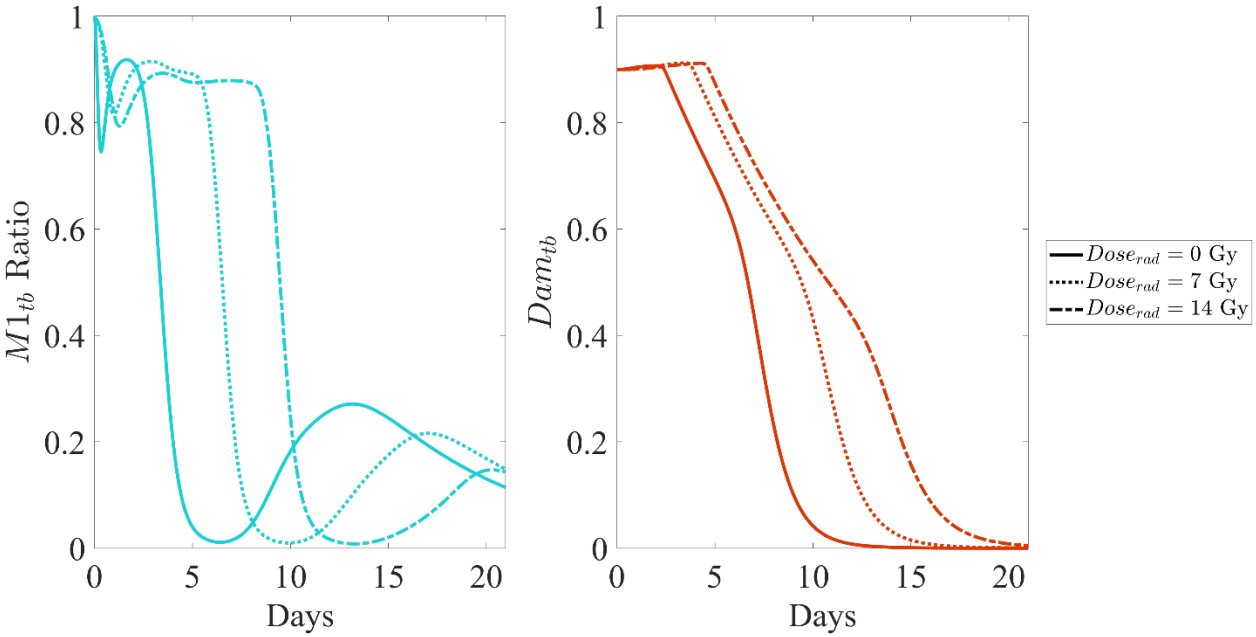

Figure 4. Plot of $M1_{tb}$ ratio and Dam_{tb} with increasing dose.

Since increased anti-inflammatory activity has only been observed at low doses of radiation and is less detrimental in acute inflammation, we only model the increase in pro-inflammatory activation observed at higher doses of radiation. To model the tendency toward pro-inflammatory macrophages at higher radiation doses, a multiplicative inhibitory term is introduced to the rate at which resting monocytes activate toward the M2 phenotype, R_{m2}. A decrease in the activation towards the anti-inflammatory phenotype will ultimately result in increased activation towards the pro-inflammatory phenotype from the resting monocyte population and create the desired polarization. The multiplicative function has the same inhibitory form as the function used to model inhibition on typical cell interactions during inflammation, $\Omega_i(R_{m2}; \overline{M}_{st}^{d}, \omega_m)$. However, in this case the function is dependent on the radiation dose to reflect that this polarization only occurs for doses larger than a critical dose value, D_{crit}. Thus, we define the function as

$$f(D) = \begin{cases} 1\,, & D < D_{crit} \\ \Omega_i\left(R_{m2}; \bar{M}_{st}^{d}, \omega_m\right), & D \geq D_{crit}. \end{cases} \tag{18}$$

Based on the literature, set $D_{crit} = 2$ Gy (Rödel et al. 2015).

3.3.4. T Lymphocytes

T lymphocytes are considered in the present model which include pro-inflammatory (i.e., γδ-T cells, TH1 cells, and TH17 cells) and anti-inflammatory (i.e., TH2 cells and regulatory T cells) phenotypes. T lymphocytes are considered to be relatively radiosensitive (United Nations Scientific Committee on the Effects of Atomic Radiation 1972; Heylmann et al. 2021) and do have resident populations in the surrounding tissue (Nguyen and Soulika 2019). Thus, T lymphocytes are also represented by populations of damaged and undamaged cells after irradiation. Again, we assume that the damaged cell population does not reproduce but can contribute to activation towards the $L1$ or $L2$ populations within the thermal burn compartment. While T lymphocytes are highly radiosensitive, their only function present in this model is general regulation of the macrophage response through inflammatory mediators, which remains unaffected by radiation. However, a damaged cell population is included for completeness. The equations for resting lymphocytes and activated lymphocytes in the burn side are given below.

$$\frac{dL_{st}^{ud}}{dt} = v(t, Dose_{rad}; \gamma_l)s_{lr} - R_{l1}L_{st}^{ud} - R_{l2}L_{st}^{ud} - d_{lr}^{ud}L_{st}^{ud} \tag{19}$$

$$\frac{dL_{st}^{d}}{dt} = -R_{l1}L_{st}^{d} - R_{l2}L_{st}^{d} - d_{lr}^{d}L_{st}^{d} \tag{20}$$

$$\frac{dL1_{tb}}{dt} = R_{l1}L_{st}^{ud} + R_{l1}L_{st}^{d} - d_l L1_{tb} \tag{21}$$

$$\frac{dL2_{tb}}{dt} = R_{l2}L_{st}^{ud} + R_{l2}L_{st}^{d} - d_l L2_{tb} \tag{22}$$

where

$$R_{l1} = \Omega_i(k_{l1}M1_{tb}; L2_{tb}, L2_1^{\infty}) \tag{23}$$

$$R_{l2} = \Omega_i(k_{l2}M2_{tb}; F_{tb}, F^{\infty}). \tag{24}$$

$$s_{lr} = \lambda_{bvtb}L_{bv} \tag{25}$$

Observe that since the ODE given by Eqn. (20) is separable, the analytical solution can be derived via an integration factor. Upon doing this, one obtains the following expression for damaged T lymphocytes in the local irradiated tissue:

$$L_{st}^{d}(t) = L_{st,0}^{d} \exp\left\{-\int_0^t R_{l1} + R_{l2} + d_{lrd}\ d\xi\right\}. \tag{26}$$

Note that ξ is a dummy variable used for integration.

3.3.5. Fibroblasts

Fibroblasts are highly proliferative (Alberts et al. 2002). As a result, they are generally radiosensitive, thus we model fibroblasts with damaged and undamaged populations in the surrounding tissue. The superficial thermal burn model considered a constant source of fibroblasts (Jennings et al. 2022a). This population is replaced by a dynamic influx from the surrounding tissues supplied by proliferative fibroblasts in the connective tissue using the term $k_{ct}F_{ct}$, which could be reduced to a constant rate, s_f. Undamaged fibroblasts in the surrounding tissue proliferate, but this is not explicitly modeled and is instead included in the constant influx from connective tissues. Damaged and undamaged fibroblasts in the surrounding tissue can then migrate to the thermal burn or decay.

Fibroblast proliferation, although largely overlapping with the inflammatory phase, is essential in signaling the resolution of inflammation and pioneering tissue repair (Velnar et al. 2009). The rapid proliferation process is necessary for the secretion of collagen and reconstruction of the extracellular matrix, which serves as a precursor to repaired tissue. Impaired fibroblast proliferation can cause a wound to progress slowly or not heal at all, resulting in persistent inflammation and continued vulnerability to infection. Irradiation has been evidenced to suppress fibroblast proliferation (Rudolph et al. 1988) and has been observed to occur in a dose-dependent manner (Chen et al. 2019).

The direct mechanism for reduced fibroblast proliferation is unclear (Rudolph et al. 1988). The observed reduction of cellular proliferation is generally assumed to be a direct decrease in proliferative abilities but could be the result of decreased survival of specific fibroblasts. Reticular fibroblasts have been shown to have a slower growth rate than papillary fibroblasts (Schafer et al. 1985) and thus an imbalance in these two populations could also result in the observed decrease in proliferation if radiosensitivity differences exist between the two populations. Regardless of the exact mechanism, a decrease in proliferation is observed (Rudolph et al. 1988). Consistent with the previous section, we use an inhibitory multiplier on the proliferation term of the fibroblast equation, $\Omega_i\left(1; F_{st}^d, \omega_f\right)$. The dependence on the population of damaged fibroblasts in the surrounding tissue allows for a dose- and time-dependent inhibitory term. Thus, the inhibition in proliferation is decreased as dose decreases and as time from injury increases. The fibroblast populations are represented by the equations below.

$$\frac{dF_{st}^{ud}}{dt} = v\left(t, Dose_{rad}; \gamma_f\right) s_f - k_{sttb}^{ud} F_{st}^{ud} - d_{fr}^{ud} F_{st}^{ud} \tag{27}$$

$$\frac{dF_{st}^{d}}{dt} = -k_{sttb}^{d} F_{st}^{d} - d_{fr}^{d} F_{st}^{d} \tag{28}$$

$$\begin{aligned}\frac{dF_{tb}}{dt} = {} & k_{sttb}^{ud} F_{st}^{ud} + k_{sttb}^{d} F_{st}^{d} \\ & + \Omega_i\left(1; F_{st}^d, \omega_f\right)\Omega_i(F_{tb}; N_{tb}, N_2^{\infty}, M1_{tb}, M1_2^{\infty})\left(k_f \right. \\ & \left. + \alpha_{dam} Dam_{tb} + \alpha_{m2} M2_{tb}\right) - d_f F_{tb}\end{aligned} \tag{29}$$

where

$$s_f = k_{ct} F_{ct}. \tag{30}$$

As we have shown with T lymphocytes, the equation for damaged fibroblasts in the surrounding tissue can be solved using separation of variables and simple integration. Additionally, since all transition rates are constant, the resultant solution is only dependent on time. The analytical solution is given by

$$F_{st}^{d}(t) = F_{st,0}^{d} e^{-\left(k_{sttb}^{d} + d_{fr}^{d}\right)t}. \tag{31}$$

3.3.6. Pathogen

Pathogens were not accounted for in the previous TDPM (Jennings et al. 2022a) as there is little to no risk of infection for superficial thermal burns (Paul et al. 2015; Abazari et al. 2020; Jeschke et al. 2020). Contrastingly, ionizing radiation is associated with a risk of infection regardless of a localized (Hill et al. 2004) or whole-body exposure (Elliott et al. 1990; Landauer et al. 2001; Ran et al. 2003; Carter et al. 2016). This risk is further elevated for irradiated burns (Ledney et al. 1991). As a result, the state variable P_{tb} describing levels of pathogens in the irradiated wound was added to the model. The ODE governing P_{tb} satisfies

$$\begin{aligned}\frac{dP_{tb}}{dt} = k_{pg}P_{tb}\left(1 - \frac{P_{tb}}{P^{\infty}}\right) - \frac{k_{pb}s_b P_{tb}}{\mu_b + k_{bp}P_{tb}} - k_{pn}P_{tb}N_{tb} - k_{pm1}P_{tb}\Omega_i(M1_{tb}; N_{tb}, N_1^{\infty}) \\ - k_{pm2}P_{tb}\Omega_i(M2_{tb}; N_{tb}, N_1^{\infty}).\end{aligned} \tag{32}$$

Following the approach of other wound healing models (Menke et al. 2010; Cooper et al. 2015; Torres et al. 2019), this ODE accounts for limited pathogen growth and removal via phagocytosis by neutrophils (N_{tb}) and macrophages ($M1_{tb}$ and $M2_{tb}$). The first term of Eqn. (32) represents logistic growth of pathogens with a carrying capacity given by P^{∞} and growth rate of k_{pg}. Note that logistic growth is widely accepted for describing exponential growth with restrictions due to competition for resources (Murray 2001; Edelstein-Keshet 2005)

The second term describes the removal of pathogens by the local background immune response, which includes mast cells and natural killer cells (Murphy and Weaver 2017). The derivation of this term, which assumes the local background immune response reaches quasi-steady state, has been described elsewhere (Reynolds et al. 2006). Parameters k_{pb}, s_b, μ, and k_{bp} capture the speed and efficiency of this response as well as how effectively it can be overwhelmed by large contamination or rapidly dividing pathogens.

The final three terms account for removal of pathogens by neutrophils and macrophages. Neutrophil activity contributes to an oxidative environment that inhibits phagocytosis by macrophages. Observe that the employed representation, including the inhibition function, parallels the phagocytosis of neutrophils by macrophages in Eqn. (8). No pathogens are removed by T lymphocytes as cytotoxic T cells are not included in the model.

The presence of pathogens in wounds activates resting neutrophils as well as resting monocytes/macrophages to the M1 phenotype (pro-inflammatory) (Broughton et al.). The terms $k_{np}P_{tb}$ and $k_{m1p}P_{tb}$ were incorporated into the activation functions for neutrophils and M1 macrophages (see Eqns. (9) and (15)). Since most pathogens do not promote the anti-inflammatory response, no modification was made to the activation terms for M2 macrophages, Eqn. (16). The model assumes that the primary function of T lymphocytes is to amplify the macrophage response. Initial activation of T lymphocytes occurs in the lymphatic tissues (Murphy and Weaver 2017). As

a result, pathogens do not appear in the activation functions for $L1_{tb}$ and $L2_{tb}$ (see Eqns. (23) and (24)).

Section 4. Numerical Simulations

Numerical simulations were performed to not only to illustrate dynamics of the TDPM governed by Eqns. (5)-(32), but also to demonstrate the model's ability to reproduce observed, known biological phenomena. Of interest to irradiated thermal burns is the time to healing. To identify this endpoint from the transients generated by the TDPM, a previous definition was adopted that states a wound is healed when Dam_{tb} is less than 0.01 (Menke et al. 2010; Jennings et al. 2022b).

All simulations were performed in MATLAB (2020).

4.1 Baseline Parameter Values and Initial Conditions

To conduct numerical simulations, baseline values for each parameter were first determined. Pointwise estimates[2] for the superficial thermal burn TDPM (Jennings et al. 2022b) served as initial values for non-radiation parameters. Similarly, due to analogous mathematical representations in the ODEs, values reported in published models were used for other unknown parameters related to pathogens and fibroblasts (Reynolds et al. 2006; Menke et al. 2010; Segal et al. 2012; Cooper et al. 2015). These initial estimates and those capturing irradiation effects were then manually calibrated so that the healing time of a minor[3] partial-thickness thermal burn occurs in 7-14 days (Abazari et al. 2020; Jeschke et al. 2020) and is delayed when radiation is added. The resulting baseline values can be found in Appendix A.

Here, a minor partial-thickness burn corresponds to $Dam_{tb}(0) = Deb_{tb}(0) = 0.9$ and $N_{tb}(0) = M1_{tb}(0) = M2_{tb}(0) = L1_{tb}(0) = L2_{tb}(0) = F_{tb}(0) = 0$; this representation has been utilized elsewhere (Creel et al. 2022; Jennings et al. 2022b). Additionally, the amount of pathogens in the burn at $t = 0$, $P_{tb}(0)$, is taken to be 0.8, which lies within the range of values employed by other mathematical models (Reynolds et al. 2006; Menke et al. 2010; Segal et al. 2012; Cooper et al. 2015).

For a given prompt radiation dose, initial conditions for the tissue-resident state variables, i.e., $\bar{M}_{st}, L_{st}$, and F_{st}, can be calculated via the LQ equation defined in Eqn. (1) as displayed in Table 2. Radiosensitive cells have lower proportions of surviving cells. For example, as suggested by the values of $p_{survival}$ shown in Table 3, tissue-resident fibroblasts are much more radiosensitive than T lymphocytes also residing in healthy tissues (e.g., regulatory T cells), while tissue-resident monocytes/macrophages are highly insensitive. Due to the large number of parameters, for $\bar{M}_{st}$, L_{st}, and F_{st}, the radiosensitivity parameters a and b satisfying the LQ equation were excluded from the manual calibration to a baseline value. Instead, the survival probabilities in Table 3 were applied directly to the initial condition assumed for thermal burn only (see Appendix A). Future work will not include making such a simplification.

[2] Here, pointwise estimates specifically refer to the representative set computed via Brute-Force with Latin-Hypercube Sampling previously reported (Jennings et al. 2022b).

[3] Minor is defined as less than 20% total body surface area (Jeschke et al. 2020).

Table 3. Survival probabilities of tissue-resident macrophages, T lymphocytes, and fibroblasts for different prompt radiation doses.

SYMBOL	$Dose_{rad}$				REFERENCES
	1 Gy	7 Gy	14 Gy	28 Gy	
$\bar{M}_{st}$	0.95	0.95	0.95	0.95	(Heylmann et al. 2021)
L_{st}*	0.8	0.3	0.3	0.3	(Geara et al. 1992; Heylmann et al. 2021)
F_{st}	0.3	0.01	0.001	0.001	(Geara et al. 1992)
* Note that at $t = 0$, L_{st} captures tissue-resident T lymphocytes, i.e., those naturally existing in healthy skin. Here, it is assumed that regulatory T-cells are the predominant subtype.					

4.2 Impaired Healing and Sustained Infection

It is well-established that radiation impairs the healing process initiated by thermal burns (Alpen et al. 1954; Ran et al. 2004; Pellmar and Ledney 2005; Iddins et al. 2022); this feature holds not only for other tissue injuries (such as soft tissue trauma and bone fracture) (United Nations Scientific Committee on the Effects of Atomic Radiation 1982; Schäffer et al. 2002; Chen et al. 2019), but also for the swath of radiation exposures from whole-body to partial-body to localized (Vegesna et al. 1993). Moreover, this delay occurs in a dose-dependent manner (United Nations Scientific Committee on the Effects of Atomic Radiation 1982; Liu et al. 2005; Chen et al. 2019; Iddins et al. 2022).

Figure 5 and 6 display the dynamics in the local irradiated tissues and burn site, respectively, as predicted by the TDPM under the baseline parameter values. In the subplots of both figures, the solid line corresponds to $Dose_{rad} = 0$, representing a non-irradiated superficial thermal burn (i.e., thermal injury only), while the non-solid lines represent an irradiated thermal burn of increasing radiation exposure for $Dose_{rad} = 1$ Gy, 7 Gy, and 14 Gy.

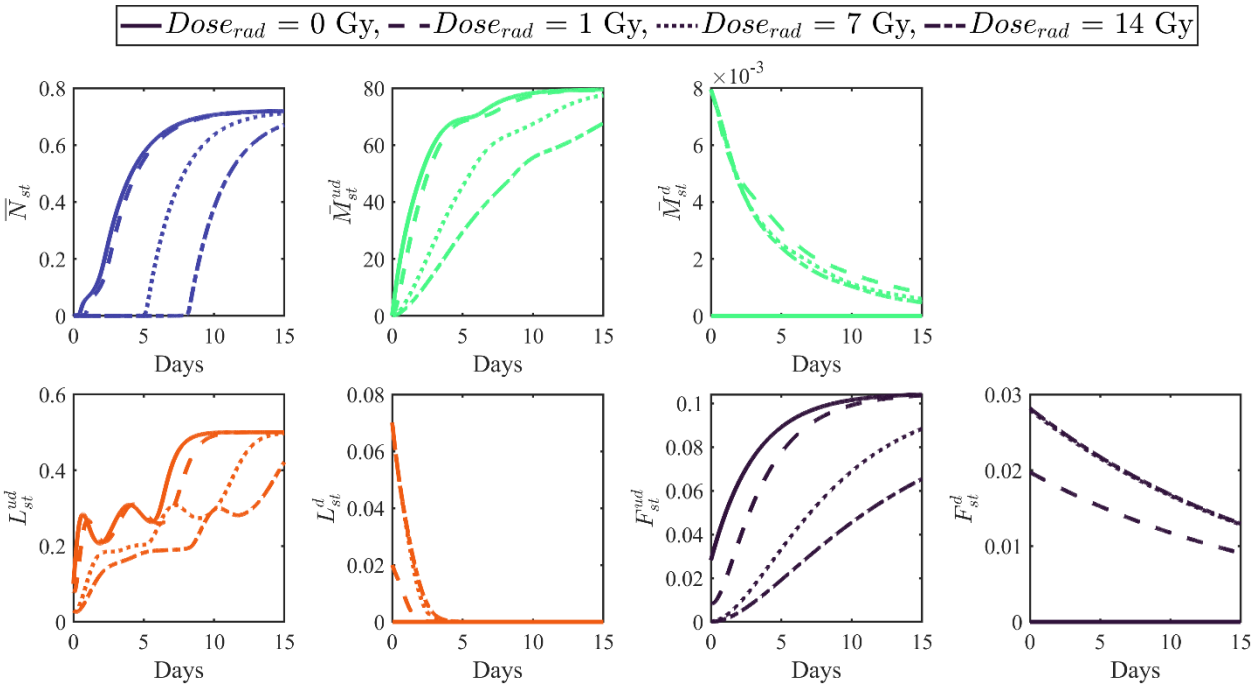

Figure 5. Baseline dynamics in the local irradiated tissue predicted by the TDPM for varying prompt localized radiation doses of increasing magnitude.

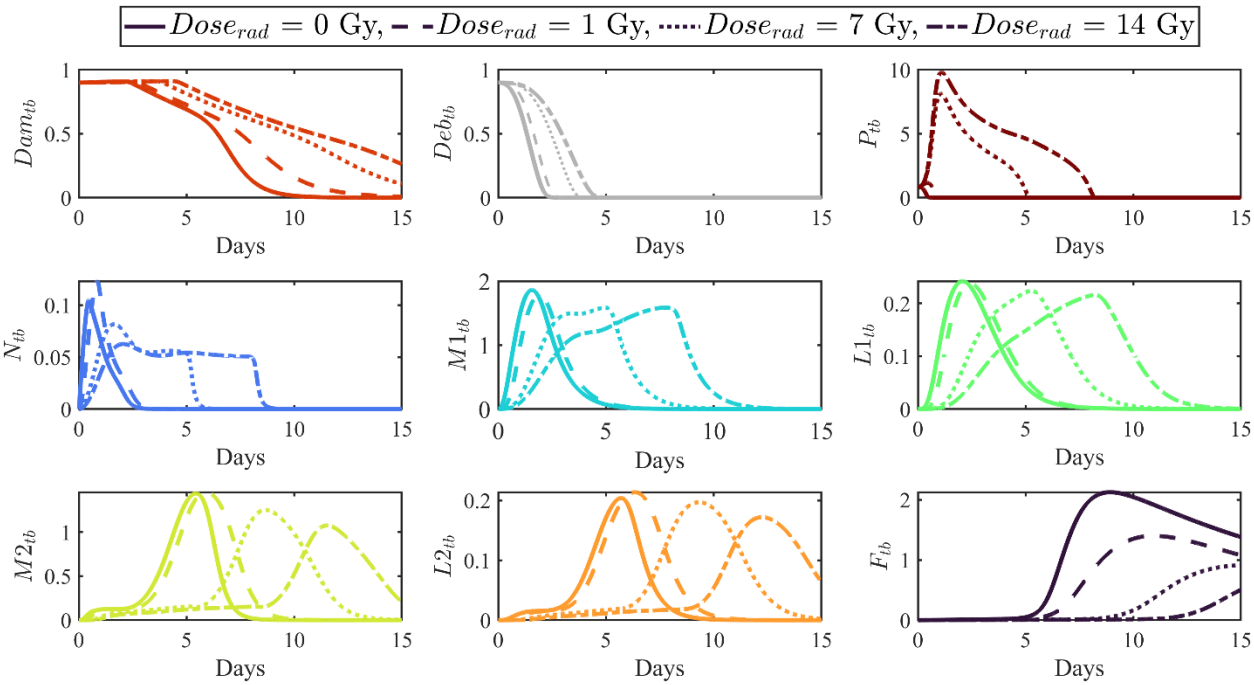

Figure 6. Baseline dynamics in the local thermal burn predicted by the TDPM for varying prompt localized radiation doses of increasing magnitude.

Visual comparisons of curves for thermal burn only against those exhibiting an irradiated burn highlight the impaired healing process for all prompt radiation doses. Further inspection reveals this disruption can be attributed to delays in undamaged cell infiltration (see the subplots for $\bar{N}_{st}$, $\bar{M}^{ud}_{st}$, L^{ud}_{st}, and F^{ud}_{st} in Figure 5), as well as additional immune stress posed by infection (see the

subplot for P_{tb} in Figure 6). The greatest effect appears to be on $\overline{N}_{st}^{ud}$, which could be due to neutrophils initiating the inflammatory process upon arrival to the wound.

Another source of the delay appears to lie with the inflammatory cascade in the burn. This can be observed in the subplots for N_{tb}, $M1_{tb}$, and, $L1_{tb}$ of Figure 6, which show that duration of the pro-inflammatory response extends with larger radiation doses. Wound healing cannot progress until the pro-inflammatory response resolves (Duffield 2003; Diegelmann and Evans 2004), thus, the model is able to mimic this mechanism when impaired healing is observed.

The subplot for Dam_{tb} in Figure 6 suggests that the time to healing increases with $Dose_{rad}$. Per the definition of "healed" employed therein (see Section 4.1), the superficial partial-thickness burn heals in 10.42, 14.74, 21.13, or 24.29 days when irradiated with 0 Gy, 1 Gy, 7 Gy, or 14 Gy, respectively. This illustrates the model's ability to capture the dose-effect relationship between healing time and radiation doses observed in published studies on irradiated thermal burns (Liu et al. 2005).

Irradiated thermal burns have been shown to be at increased risk of secondary infection (Ledney et al. 1991; Kiang et al. 2010b). The dynamics for P_{tb} predicted by the TDPM displayed in Figure 6 show that both the magnitude and duration of pathogens present in the wound increases as $Dose_{rad}$ increases. In other words, for low doses, inflammatory cells can quickly remove pathogens (via phagocytosis) at the burn site; however, for a higher dose radiation exposure, these cells are unable to control the pathogen population in the time immediately following insult, not only in terms of abundance but also duration, allowing for pathogens to persist for an extended period. This dovetails with the documented increased risk of infection by other studies mentioned above.

4.3 Radiation-Induced Inhibition

4.3.1. Immune Cell Infiltration

Next, consider a minor superficial thermal burn irradiated with 14 Gy. Assuming the initial amount of pathogen at the burn site is the same as that in Section 4.1, the time to healing predicted by the model is 24.29 days. To verify the impact of radiation-induced impaired infiltration into the wound site, each γ as defined by Eqn. (4) was increased by a factor of 100-200 while all other parameters remain fixed at their baseline values. Recall that an increase to γ_c means that state variable c returns to its non-irradiated infiltration rate much faster. Thus, the baseline case represents the situation in which the same prompt radiation dose (14 Gy) delays the infiltration of immune cells and fibroblasts into the site of injury.

Figure 7 and Figure 8 compare transients generated by the TDPM at baseline with those where a variable-specific infiltration inhibition is mitigated to some degree. As expected, the effect of γ_c is greatest on the corresponding state variable c; for example, $\overline{N}_{st}$ starts increasing earliest when γ_n is varied. Moreover, the increase to each γ results in damage that is more rapidly repaired - albeit to varying degrees - in comparison to the baseline (see the subplot for Dam_{tb} in Figure 8). Specifically, for γ_n, γ_m, γ_l, and γ_f, the healing time decreased from 24.29 days at baseline to 23.79, 21.53, 23.09, and 23.05 days, respectively. The greatest reduction in healing time occurs when monocyte/macrophage infiltration is improved despite irradiation. However, given that inflammation and proliferation require complex coordination across a range of specialized and

somewhat competing biological processes, it is not surprising that improving infiltration by a single variable would fail to dramatically speed up healing.

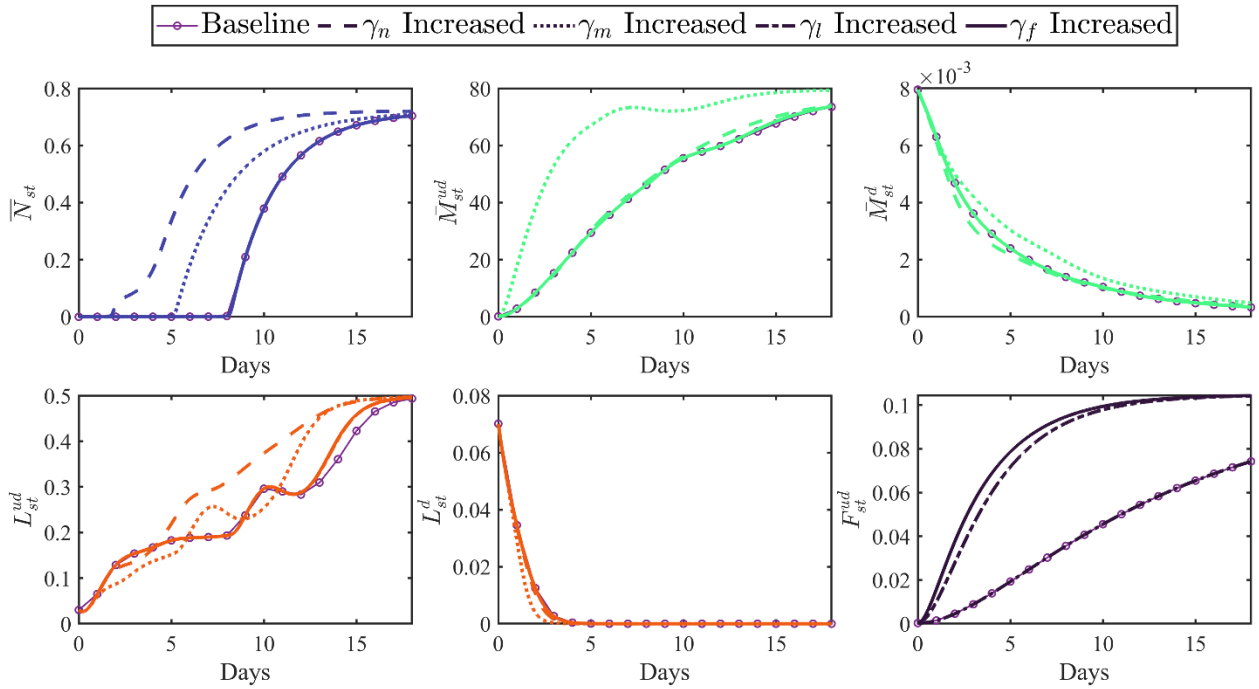

Figure 7. Comparison of inflammation and repair dynamics in the local irradiated tissue produced by the TDPM for varying degrees of radiation-induced infiltration inhibition.

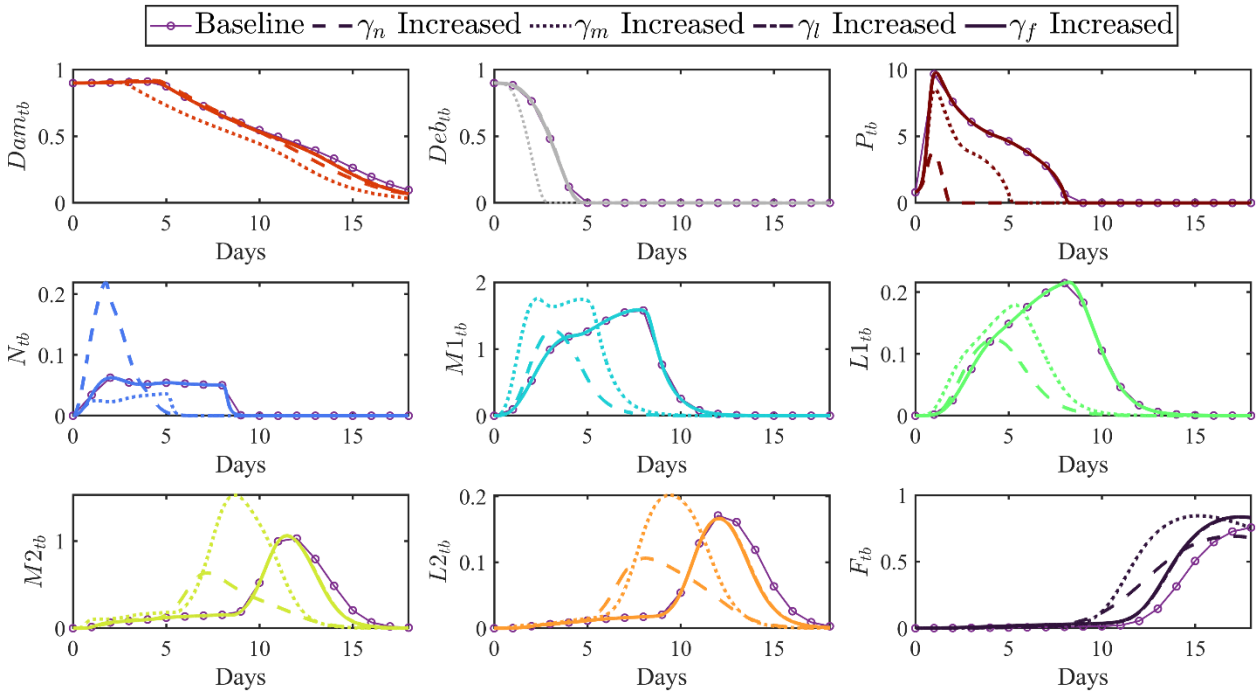

Figure 8. Comparison of inflammation and repair dynamics in the local thermal burn produced by the TDPM for varying degrees of radiation-induced infiltration inhibition.

4.3.2. Fibroblast Dysfunction

Consider the same irradiated partial-thickness thermal burn discussed above. To examine the impact of radiation-induced fibroblast dysfunction, simulations were conducted varying parameters ω_{dam} and ω_f individually, then jointly. An increase in ω_{dam} and/or ω_f by a factor of 100-200 equates to shortening of the radiation-associated inhibition period on fibroblast proliferation and collagen deposition, allowing each to return more quickly to their non-irradiated levels.

Figure 9 displays results from comparing the transients predicted by the TDPM when fibroblast dysfunction caused by irradiation is mitigated as compared to the effect at baseline. Only results are shown for Dam_{tb} and F_{tb} as the inhibitory effects of ω_{dam} and ω_f occur during the proliferation phase, which can only commence once inflammation has resolved. Thus, changes to these parameters - by design - will be concentrated to Dam_{tb} and F_{tb}.

As suggested by the subplot for Dam_{tb}, the greatest reduction in the time to healing occurs when both ω_{dam} and ω_f were increased (24.29 days to 18.68 days). However, the irradiated wound healed within 19.42 days when fibroblast proliferation was impaired only for a shorter period (i.e., ω_f increased). This is not surprising, since improved proliferation will increase F_{tb}, which in turn will reduce Dam_{tb}. Fibroblast dysfunction has proven to be a very important component of radiation injury (Rudolph et al. 1988; Vegesna et al. 1993; Schäffer et al. 2002; Jadhav et al. 2013; Chen et al. 2019) and the model is able to display this as increased healing times for increasing inhibition of fibroblast function.

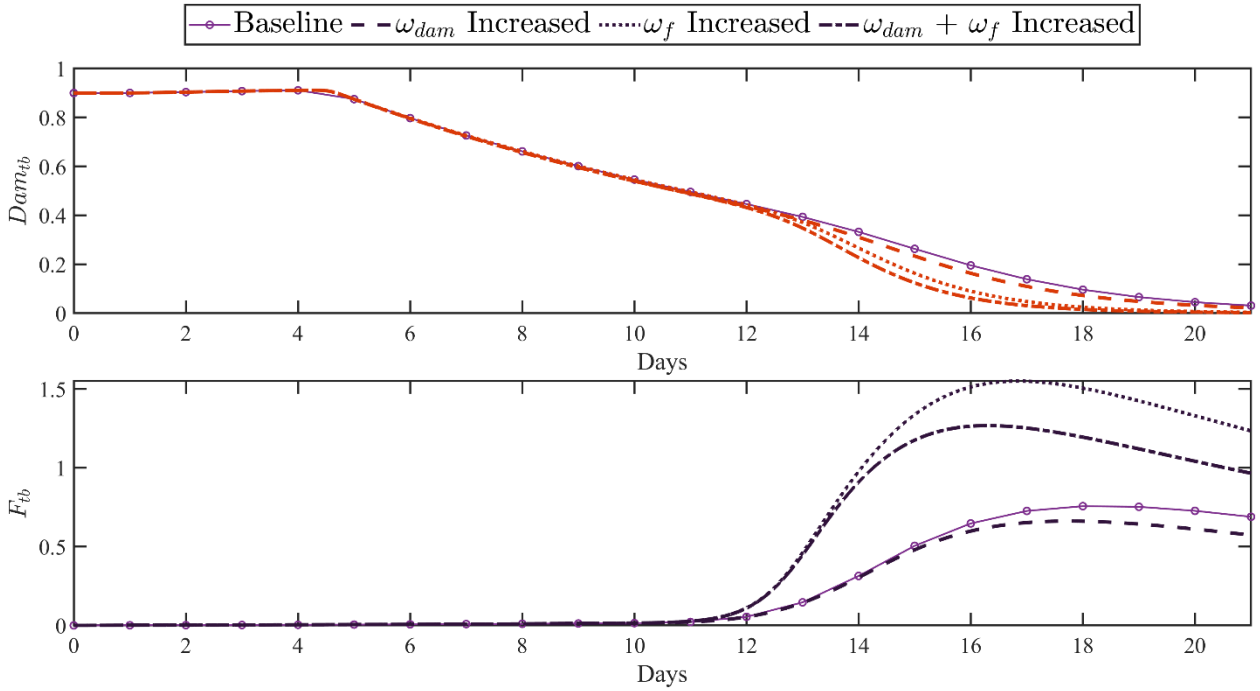

Figure 9. Comparison of repair dynamics in the local thermal burn produced by the TDPM for varying degrees of radiation-induced fibroblast dysfunction.

Section 5. Discussion

Ionizing radiation has the capacity to injure a considerable number of tissues in the body, presenting a formidable challenge for capturing its effects in a mathematical model. To advance the development of mechanistic, time-dependent mathematical models of combined injury (here thermal and ionizing radiation) in a well-posed and systematic manner, we first considered the effects of localized ionizing radiation and superficial thermal burns. In terms of burn severity, we focused on survivable injuries with little to no medical intervention, as these would be most likely to occur in survivors of a NUDET event. Additionally, localized, or partial-body, irradiation is relevant to military personnel. Protection provided by armor and other military equipment would shield most of the body from irradiation and likely localize injury to the hands, face, and neck. However, these areas are considered particularly sensitive regions to receive thermal burns and radiation injury (Reeves 2018; DiCarlo et al. 2020). The overall goal of the combined injury model for DTRA is to predict combat readiness for a soldier receiving injuries from a NUDET event as well as medical planning. For this reason, we only consider characteristics relevant to military personnel such as the use of localized radiation injury, as well as population assumptions regarding age and sex. Potential future models could consider whole-body irradiation, which would affect the hematopoietic and gastrointestinal systems, as well as other physiological processes and modifications made for age and sex to encompass a civilian population.

It is well-established that inflammation is a common pathway for injuries resulting from exposure to more than one insult (Kiang et al. 2010b, 2012, 2015; Probst et al. 2012; Mangum et al. 2019; Stewart et al. 2019; Land 2020). The previously developed TDPM on inflammation and early fibroblast activity initiated by superficial thermal injuries was modified to incorporate localized irradiation effects in the wound site. Enhancements to the model included diminished immune cell infiltration to the wound site due to radiation-induced vascular damage; polarization of macrophages to a pro-inflammatory phenotype for doses above 2 Gy; impaired fibroblast proliferation and repair (due to reduced or irregular collagen deposition); and contamination of the wound by pathogens. Moreover, to the authors best knowledge, the TDPM is the first of its kind, as there is not another existing model describing healing of an irradiated thermal burn.

Numerical simulations showed that the model can reproduce known timings of immune cell infiltration as well as the onset of fibroblast proliferation for a non-irradiated burn, demonstrating the model's ability to capture delayed healing in a dose-dependent manner. The inclusion of irradiation effects produced known delays in the infiltration of immune cells, delays in fibroblast proliferation, and impaired removal of damage due to irregular collagen deposition. Additionally, the introduction of pathogen into the system further delayed wound healing and provided the opportunity for pathogen overgrowth and sustained infection. These delays prevent the normal progression of healing, rendering personnel susceptible to secondary infections or additional complications from sustained inflammation.

Current model parameters were manually calibrated to exhibit qualitative dynamics but require quantitative estimation. Future steps include fitting the model to available data to provide numerical markers of model efficacy. The availability of data poses an additional challenge, as human data is sparse and observational. Historical NUDET events and nuclear accidents provide the only source of human data and specific variables such as radiation dose are unknown or poorly estimated. Animal models provide a larger resource of experimentally controlled data, but special considerations do need

to be made to ensure the data can be applied to human models. Large porcine (e.g., Yorkshire pig) models have been shown to exhibit similar characteristics to human skin and have been used in radiation skin research since the 1980s (DiCarlo et al. 2020). Other models such as the Göttingen minipig and murine models have also been used. While porcine models have been demonstrated to be most applicable to human subjects for skin injury, murine models are much more prevalent in research due to availability and cost. However, differences do exist in some cell types and processes. For T lymphocytes, the dominant population in murine skin is γδ-T cells and the dominant population in human skin is αβ T cells. These cells differ in their predominant cytokines and overall role in the immune response. Additionally, human blood is significantly neutrophil-rich (50-70%) whereas murine blood is significantly lymphocyte-rich (75-90%) (Doeing et al. 2003). Despite these differences, murine models can still offer important insight into human models and serve as a rich source of data for radiation combined injuries (Doeing et al. 2003).

Conclusions drawn from *in vitro* experimental designs also warrant some scrutiny. Observations made *in vitro* are not always applicable to an *in vivo* model. For instance, *in vitro* macrophages derived from mesenchymal cells in the bone marrow can generate different responses from tissue macrophages obtained *in vivo*. Human macrophages also take longer to respond to stimulatory factors, and it is postulated that some *in vitro* experiments may have ended before a response could be detected. Other differences exist based on macrophage source have also been summarized (Thomas and Mattila 2014). Again, these studies still prove to be useful and provide an abundant source of data to test experimental hypotheses, but potential dissimilarities need to be considered to obtain accurate estimates of the parameters and ensure adaptability to human subjects. Future efforts on the current model will include this endeavor.

Section 6. Future Models & Potential Impacts

The current model focuses on combined injury defined by the combination of a thermal burn and radiation injury, but other insults from a NUDET event exist. Injuries obtained directly or indirectly from the blast wave (i.e., bone fractures, crush injuries, pulmonary blast injury, hemorrhage, etc.) also warrant discussion. In fact, victims closest to the hypocenter are expected to also sustain injuries from blast, burns, and external body radiation (Brooks et al. 1952). For those that survive, the addition of another injury inflicts increased stress on the immune response and introduces additional complexities. Current efforts at ARA include the development of a bone fracture model that will later be incorporated into a combined model with thermal burns and radiation. Like the effects of whole-body irradiation, a bone fracture of a certain severity can disrupt the hematopoietic system, thus eliminating our current assumptions that hematopoietic sources of cells are constant. This injury presents an additional complication in modeling combined injury and an increase in model complexity. Therefore, future models are expected to be sizable (in terms of both number of equations and parameters) as we attempt to replicate the complex dynamics of combined injury. Despite concerns regarding the enormity of these models, these TDPMs of combined injury will eventually provide increasingly accurate predictions for combat readiness as well as the opportunity for specialized predictions tailored to distinct combinations and intensities of injuries.

Section 7. References

Abazari M, Ghaffari A, Rashidzadeh H, Badeleh SM, Maleki Y. A systematic review on classification, identification, and healing process of burn wound healing. Int J Low Extrem Wounds 1–13; 2020.

Alberts B, Johnson A, Lewis J, Raff M, Roberts K, Walter P. Fibroblasts and their transformations: The connective-tissue cell family. In: Molecular Biology of the Cell. 4th ed. New York: Garland Science; 2002.

Alpen EL, Sheline GE, Francisco S. The combined effects of thermal burns and whole body irradiation on survival time and mortality. Ann Surg 140:113–118; 1954.

Beauford SS, Kumari A, Garnett-Benson C. Ionizing radiation modulates the phenotype and function of human CD4+ induced regulatory T cells. BMC Immunol 21:1–13; 2020.

Bentzen SM, Thames HD, Overgaard M. Latent-time estimation for late cutaneous and subcutaneous radiation reactions in a single-follow-up clinical study. Radiother Oncol 15:267–274; 1989.

Brenner DJ. Point: The linear-quadratic model is an appropriate methodology for determining iso-effective doses at large doses per fraction. Semin Radiat Oncol 18:234–239; 2008.

Brooks JW, Evans EI, Ham WT, Reid JD. The influence of external body radiation on mortality from thermal burns. Ann Surg 136:533–545; 1952.

Broughton GI, Jeffrey Janis UE, Attinger CE. The Basic Science of Wound Healing.

Carter SR, Chen MM, Palmer JL, Wang L, Ramirez L, Plackett TP, Gamelli RL, Kovacs EJ. Neutrophil accumulation in the small intestine contributes to local tissue destruction following combined radiation and burn injury. J Burn Care Res 37:97–105; 2016.

Chadwick KH, Leenhouts HP. A molecular theory of cell survival. Phys Med Biol 18:78–87; 1973.

Chen Y, Sun X, Peng Y, Eichenbaum JV, Ren L, Liu Y. Effects of different radiation sources on the performance of collagen-cased corneal repair materials and macrophage polarization. ACS omega 7:22559–22566; 2022.

Chen Y, Zhang Q, Wu Y, Branch-Brooks CD, Butler CE. Short-term influences of radiation on musculofascial healing in a laparotomy rat model. Sci Rep 9:1–11; 2019.

Cheng T, Chen Z, Yan Y, Ran X, Su Y, AI G. Experimental studies on the treatment and pathological basis of combined radiation and burn injury. Chin Med J (Engl) 115:1763–1766; 2002.

Chow CC, Clermont G, Kumar R, Lagoa C, Tawadrous Z, Gallo D, Betten B, Bartels J, Constantine G, Fink MP, Billiar TR, Vodovotz Y. The acute inflammatory response in diverse shock states. Shock 24:74–84; 2005.

Clarke RH, Dunster HJ, Guskova AK, Jacobi W, Li D, Liniecki J, Meinhold CB, Mettler F, Shigematsu I, Silini G, Sinclair WK, Lindell B, Morgan KZ, Taylor LS. Annals of the ICRP. Ann ICRP 22:1; 1991.

Cooper RL, Segal RA, Diegelmann RF, Reynolds AM. Modeling the effects of systemic mediators on

the inflammatory phase of wound healing. J Theor Biol 367:86–99; 2015.

Creel A, Jennings R, Reynolds A. Sensitivity Analysis for a Time-Dependent Physiological Model of Superficial Thermal Burns. DTRA-TR-21-063 R1, Defense Threat Reduction Agency, Fort Belvoir, VA; 2022.

Curtis SB. Lethal and potentially lethal lesions induced by radiation- A unified repair model. Radiat Res Soc 106:252–270; 1986.

Day JD, Metes DM, Vodovotz Y. Mathematical modeling of early cellular innate and adaptive immune responses to ischemia/reperfusion injury and solid organ allotransplantation. Front Immunol 6; 2015.

Deloch L, Fuchs J, Rückert M, Fietkau R, Frey B, Gaipl U. Low-dose irradiation differentially impacts macrophage phenotype in dependence of fibroblast-like synoviocytes and radiation dose. J Immunol Res 2019; 2019.

DiCarlo AL, Bandremer AC, Hollingsworth BA, Kasim S, Laniyonu A, Todd NF, Wang SJ, Wertheimer ER, Rios CI. Cutaneous radiation injuries: Models, assessment and treatments. Radiat Res 194:315–344; 2020.

DiCarlo AL, Hatchett RJ, Kaminski JM, Ledney GD, Pellmar TC, Okunieff P, Ramakrishnan N. Medical countermeasures for radiation combined injury: radiation with burn, blast, trauma and/or s epsis. Report of an NIAID Workshop, March 26–27, 2007. Radiat Res 169:712–721; 2008.

DiCarlo AL, Maher C, Hick JL, Hanfling D, Dainiak N, Chao N, Bader JL, Coleman CN, Weinstock DM. Radiation injury after a nuclear detonation: Medical consequences and the need for scarce resources allocation. Disaster Med Public Health Prep 5; 2011.

Diegelmann RF, Evans MC. Wound Healing: An overview of acute, fibrotic and delayed healing. Front Biosci 9:283–289; 2004.

Doeing DC, Borowicz JL, Crockett ET. Gender dimorphism in differential peripheral blood leukocyte counts in mice using cardiac, tail, foot, and saphenous vein puncture methods. BMC Clin Pathol 3:1–6; 2003.

Dormand EL, Banwell PE, Goodacre TEE. Radiotherapy and wound healing. Int Wound J 2:112–127; 2005.

Duffield JS. The inflammatory macrophage: A story of Jekyll and Hyde. Clin Sci 104:27–38; 2003.

Edelstein-Keshet L. Mathematical Models in Biology. Math Model Biol; 2005.

Elliott TB, Brook I, Stiefel SM. Quantitative study of wound infection in irradiated mice. Int J Radiat Biol 58:341–350; 1990.

Evers LH, Bhavsar D, Mailänder P. The biology of burn injury. Exp Dermatol 19:777–783; 2010.

Geara F, Peters L, Kian Ang K, Wike J, Sivon S, Guttenberger R, Callender D, Malaise E, Brock W. Intrinsic radiosensitivity of normal human fibroblasts and lymphocytes after high- and low-dose-rate irradiation. Cancer Res 52:6348–6352; 1992.

Goodhead DT. Saturable repair models of radiation action in mammalian cells. Radiat Res 104:58–67;

1985.

Gu Q, Wang D, Gao Y, Zhou J, Peng R, Cui Y, Xia G, Qing Q, Yang H, Liu J, Zhao M. Expression of MMP1 in Surgical and Radiation-Impaired Wound Healing and Its Effects on the Healing Process. J Environ Pathol Toxicol Oncol 21:71–78; 2002.

Hall E, Giaccia A. Radiobiology for the Radiobiologist. 7th ed. Philadelphia: Wolters Kluwer/Lippincott Williams and Wilkins; 2012.

Hanin L, Zaider M. A mechanistic description of radiation-induced damage to normal tissue and its healing kinetics. Phys Med Biol 58:825–839; 2013.

Heylmann D, Ponath V, Kindler T, Kaina B. Comparison of DNA repair and radiosensitivity of different blood cell populations. Sci Rep 11:1–13; 2021.

Hill A, Hanson M, Bogle MA, Duvic M. Severe radiation dermatitis is related to Staphylococcus aureus. Am J Clin Oncol 27:361–363; 2004.

Iddins CJ, Dicarlo AL, Ervin MD, Herrera-Reyes E, Goans RE. Cutaneous and local radiation injuries. J Radiol Prot 42:1–38; 2022.

Iijima S. Pathology of atomic bomb casualties. Acta Pathol Japan 32; 1982.

Jadhav SS, Sharma N, Meeks CJ, Mordwinkin NM, Espinoza TB, Roda NR, Dizerega GS, Hill CK, Louie SG, Rodgers KE. Effects of combined radiation and burn injury on the rennin-angiotensin system. Wound Repair Regen 21:131–140; 2013.

Jennings R, Creel A, Reynolds A. A Time-Dependent Physiological Model of Innate and Adaptive Immune Responses Activated by Superficial Thermal Burns. DTRA-TR-21-032 R1, Defense Threat Reduction Agency, Fort Belvoir, VA; 2022a.

Jennings R, Creel A, Reynolds A. Estimation of Inflammation and Repair Parameters for a Superficial Thermal Burn. DTRA-TR-22-026, Defense Threat Reduction Agency, Fort Belvoir, VA; 2022b.

Jeschke MG, van Baar ME, Choudhry MA, Chung KK, Gibran NS, Logsetty S. Burn injury. Nat Rev Dis Prim 6; 2020.

Jo WS, Kang S, Jeong SK, Bae MJ, Lee CG, Son Y, Lee HJ, Jeong MH, Kim SH, Moon C, Shin IS, Kim JS. Low dose rate radiation regulates M2-like macrophages in an allergic airway inflammation mouse model. Dose-Response 20:1–12; 2022.

Joiner MC. Chapter 4: Quantifying cell kill and cell survival. In: Joiner MC and Kogel AJ van der, eds. Basic Clinical Radiobiology. 5th ed. Boca Raton, FL: Taylor & Francis Group; 2018:31–43.

Kiang JG, Garrison BR, Burns TM, Zhai M, Dews IC, Ney PH, Cary LH, Fukumoto R, Elliott TB, Ledney GD. Wound trauma alters ionizing radiation dose assessment. Cell Biosci 2; 2012.

Kiang JG, Garrison BR, Gorbunov N V. Radiation combined injury: DNA damage, apoptosis, and autophagy. Adapt Med 2:1–10; 2010a.

Kiang JG, Jiao W, Cary LH, Mog SR, Elliott TB, Pellmar TC, Ledney GD. Wound trauma increases radiation-induced mortality by activation of iNOS pathway and elevation of cytokine concentrations and bacterial infection. Radiat Res 173:319–332; 2010b.

Kiang JG, Smith JT, Anderson MN, Swift JM, Christensen CL, Gupta P, Balakathiresan N, Maheshwari RK. Hemorrhage exacerbates radiation effects on survival, leukocytopenia, thrombopenia, erythropenia, bone marrow cell depletion and hematopoiesis, and inflammation-associated microRNAs expression in kidney. PLoS One 10:e0139271; 2015.

Kishi H. Effects of the 'special bomb': Recollections of a neurosurgeon in Hiroshima, August 8-15, 1945. Neurosurgery 47:441–446; 2000.

Kuang Y, Nagy JD, Eikenberry SE. Introduction to Mathematical Oncology. New York, NY: Chapman and Hall/CRC; 2016.

Land WG. Chapter 8: DAMP-controlled and uncontrolled responses to trauma: Wound healing and polytrauma. In: Damage-Associated Molecular Patterns in Human Diseases, Volume 2: Danger Signals as Diagnostics, Prognostics, and Therapeutic Targets. Springer International Publishing; 2020:279–335.

Landauer MR, Elliott TB, King GL, Samy Bouhaouala S, Wilhelmsen C, Ferrell JL, Wang PS, Chap A, Knudson GB. Performance decrement after combined exposure to ionizing radiation and Shigella sonnei. Mil Med 166; 2001.

Ledney GD, Madonna GS, Elliott TB, Moore MM, Jackson WE. Therapy of infections in mice irradiated in mixed neutron/photon fields and inflicted with wound trauma: A review of current work. Radiat Res 128:S18–S28; 1991.

Lewin TD, Maini PK, Moros EG, Enderling H, Byrne HM. The evolution of tumour composition during fractionated radiotherapy: Implications for outcome. Bull Math Biol 80:1207–1235; 2018.

Liu X, Liu J-Z, Zhang E, Li P, Zhou P, Cheng TM, Zhou YG. Impaired wound healing after local soft x-ray irradiation in rat skin: Time course study of pathology, proliferation, cell cycle, and apoptosis. J Trauma Inj Infect Crit Care 59:682–690; 2005.

Mangum LH, Avila JJ, Hurtgen BJ, Lofgren AL, Wenke JC. Burn and thoracic trauma alters fracture healing, systemic inflammation, and leukocyte kinetics in a rat model of polytrauma. J Orthop Surg Res 14:1–15; 2019.

McMahon S. The linear quadratic model: Usage, interpretation and challenges. Phys Med Biol 64:01TR01; 2019.

Menke NB, Cain JW, Reynolds A, Chan DM, Segal RA, Witten TM, Bonchev DG, Diegelmann RF, Ward KR. An in silico approach to the analysis of acute wound healing. Wound Repair Regen 18:105–113; 2010.

Minucci S, Heise RL, Valentine MS, Kamga Gninzeko FJ, Reynolds AM. Mathematical modeling of ventilator-induced lung inflammation. J Theor Biol 526; 2021.

Mosser DM, Edwards JP. Exploring the full spectrum of macrophage activation. Nat Rev Immunol 8:958–969; 2008.

Murphy K, Weaver C. Janeway's Immunobiology. Garland Science. 2017.

Murray JD. Mathematical Biology: I. An Introduction, Third Edition. Springer; 2001.

Nguyen A V., Soulika AM. The dynamics of the skin's immune system. Int J Mol Sci 20:1811; 2019.

Palmer JL, Deburghgraeve CR, Bird MD, Hauer-Jensen M, Kovacs EJ. Development of a combined radiation and burn injury model. J Burn Care Res 32:317–323; 2011.

Paul F, Arkin Y, Giladi A, Jaitin D, Kenigsberg E, Keren-Shaul H, Winter D, Lara-Astiaso D, Gury M, Weiner A, David E, Cohen N, Lauridsen FKB, Haas S, Schlitzer A, Mildner A, Ginhoux F, Jung S, Trumpp A, Porse B, Tanay A, Amit I. Transcriptional heterogeneity and lineage commitment in myeloid progenitors. Cell 163:1663–1677; 2015.

Pellmar TC, Ledney GD. Combined injury: Radiation in combination with trauma, infectious disease, or chemical exposures. Nato-Rtg-099 1–9; 2005.

Pinto A, Pinto M, Cardoso A, Monteiro C, Pinto M, Maia A, Castro P, Figueira R, Monteiro A, Marques M, Mareel M, Gomes Dos Santos S, Seruca R, Barbosa M, Rocha S, Oliveira M. Ionizing radiation modulates human macrophages towards a pro-inflammatory phenotype preserving their pro-invasive and pro-angiogenic capacities. Sci Rep 6:18765; 2016.

Probst C, Mirzayan MJ, Mommsen P, Zeckey C, Tegeder T, Geerken L, Maegele M, Samii A, Van Griensven M. Systemic inflammatory effects of traumatic brain injury, femur fracture, and shock: An experimental murine polytrauma model. Mediators Inflamm 2012:2–9; 2012.

Qu J, Cheng T, Shi C, Lin Y, Ran X. A study on the activity of fibroblast cells in connection with tissue recovery in the wounds of skin injury after whole-body irradiation. J Radiat Res 45:341–344; 2004.

Ran X, Cheng T, Lin Y, Qu J, Liu D, AI G, Yan G, Wang W, Xu R. Dose-effect relationships in total body irradiation on the healing of cutaneous wounds. Chin Med J (Engl) 116:878–882; 2003.

Ran X, Cheng T, Shi C, Xu H, Qu J, Yan G, Su Y, Wang W, Xu R. The effects of total-body irradiation on the survival and skin wound healing of rats with combined radiation-wound injury. J Trauma - Inj Infect Crit Care 57:1087–1093; 2004.

Reeves GI. Chapter 14: Effects on Personnel. In: EM-1: Capabilities of Nuclear Weapons. DTRA-EM-1-CH-14 (R1), Defense Threat Reduction Agency, Fort Belvoir, VA; 2018.

Reynolds A, Rubin J, Clermont G, Day J, Vodovotz Y, Bard Ermentrout G. A reduced mathematical model of the acute inflammatory response: I. Derivation of model and analysis of anti-inflammation. J Theor Biol 242:220–236; 2006.

Rödel F, Frey B, Manda K, Hildebrandt G, Hehlgans S, Keilholz L, Seegenschmiedt MH, Gaipl US, Rödel C. Immunomodulatory properties and molecular effects in inflammatory diseases of low-dose x-irradiation. Front Oncol 2; 2012.

Rödel F, Frey B, Multhoff G, Gaipl U. Contribution of the immune system to bystander and non-targeted effects of ionizing radiation. Cancer Lett 356:105–113; 2015.

Rudolph R, Berg J Vande, Schneider JA, Fisher JC, Poolman WL. Slowed growth of cultured fibroblasts from human radiation wounds. Plast Reconstr Surg 82:669–675; 1988.

Ryan JL. Ionizing radiation: The good, the bad, and the ugly. J Invest Dermatol 132:985–993; 2012.

Schafer IA, Pandy M, Ferguson R, Davis BR. Comparative observation of fibroblasts derived from the papillary and reticular dermis of infants and adults: Growth kinetics, packing density at confluence and surface morphology. Mech Ageing Dev 31:275–293; 1985.

Schäffer M, Weimer W, Wider S, Stülten C, Bongartz M, Budach W, Becker HD. Differential expression of inflammatory mediators in radiation-impaired wound healing. J Surg Res 107:93–100; 2002.

Segal RA, Diegelmann RF, Ward KR, Reynolds A. A differential equation model of collagen accumulation in a healing wound. Bull Math Biol 74:2165–2182; 2012.

Shi X, Shiao SL. The role of macrophage phenotype in regulating the response to radiation therapy. Transl Res 191:64–80; 2018.

Smirnova OA. Comparative analysis of the dynamics of thrombocytopoietic, granulocytopoietic, and erythropoietic systems in irradiated humans: A modeling approach. Health Phys 103:787–801; 2012.

Stewart L, Shaikh F, Bradley W, Lu D, Blyth DM, Petfield JL, Whitman TJ, Krauss M, Greenberg L, Tribble DR. Combat-related extremity wounds: Injury factors predicting early onset infections. Mil Med 184:83–91; 2019.

Stromberg LW, Woodward KT, Mahin DT, Donati RM. Combined surgical and radiation injury the effect of timinig of wounding and whole body gamma irradiation on 30 Day mortality and rate of wound contracture in the rodent. Comb Surg Radiat Inj 167; 1967.

Sweeney JF, Nguyen PK, Omann GM, Hinshaw DB. Ultraviolet irradiation accelerates apoptosis in human polymorphonuclear leukocytes: protection by LPS and GM-CSF. J Leukoc Biol 62:517–523; 1997.

Thomas AC, Mattila JT. 'Of mice and men': Arginine metabolism in macrophages. Front Immunol 5:1–7; 2014.

Torres M, Wang J, Yannie PJ, Ghosh S, Segal RA, Reynolds AM. Identifying important parameters in the inflammatory process with a mathematical model of immune cell influx and macrophage polarization. PLoS Comput Biol 15:e1007172; 2019.

United Nations Scientific Committee on the Effects of Atomic Radiation. Ionizing Radiation, Levels and Effects, United Nations Scientific Committee on the Effects of Atomic Radiation (UNSCEAR) 1972 Report: Report to the General Assembly, with Scientific Annexes. 1972.

United Nations Scientific Committee on the Effects of Atomic Radiation. Ionizing Radiation, Sources and Biological Effects, United Nations Scientific Committee on the Effects of Atomic Radiation (UNSCEAR) 1982 Report: Report to the General Assembly, with Scientific Annexes. 1982.

United Nations Scientific Committee on the Effects of Atomic Radiation. Effects of Ionizing Radiation, United Nations Scientific Committee on the Effects of Atomic Radiation (UNSCEAR) 2006 Report, Volume II: Scientific Annexes C, D, and E. 2006.

Vegesna V, Withers HR, Holly FE, McBride WH. The effect of local and systemic irradiation on impairment of wound healing in mice. Radiat Res 135:431–433; 1993.

Velnar T, Bailey T, Smrkolj V. The wound healing process: An overview of the cellular and molecular mechanisms. J Int Med Res 37:1528–1542; 2009.

Wentz J, Oldson D, Stricklin D. Models of Hematopoietic Dynamics Following Burn for Use in Combined Injury Simulations. DTRA-TR-15-024, Defense Threat Reduction Agency, Fort Belvoir, VA; 2015.

Yan Y, Ran X, Wei S. Changes of immune functions after radiation, burns and combined radiation-burn injury in rats. Chin Med J (Engl) 10:85–89; 1995.

Zawaski JA, Yates R, Miller DD, Kaffes CC. Radiation combined injury models to study the effects of interventions and wound biomechanics. Radiat Res 182:640–652; 2014.

Zelman D, Porteous DD, Bromberg BE. The effect of total body irradiation on wound healing and the hematopoietic system in mice. Bull N Y Acad Med 45:293–300; 1968.

MATLAB 2020b. The MathWorks, Inc., Natick, MA, U.S.A.; 2020.

Appendix A. Parameter Symbols, Definitions, Biological Units, and Baseline Values

PARAMETER		DESCRPTION	UNITS	BASELINE
Inhibition (non-radiation related)	Deb_{dam}^{∞}	Constant controlling the effectiveness of Deb_{tb} at inhibiting damage repair	D-units	0.01
	Deb_H	Constant controlling the effectiveness of Deb_{tb} at inhibiting phagocytic removal of debris by N_{tb}, $M1_{tb}$ and $M2_{tb}$	D-units	0.061
	N_1^{∞}	Constant controlling the effectiveness of N_{tb} at inhibiting the activity on other immune cells	N-units	0.1417
	N_2^{∞}	Constant controlling the effectiveness of N_{tb} at inhibiting proliferation and activation of F_{tb}	N-units	0.1
	$M1_1^{\infty}$	Constant controlling the effectiveness of $M1_{tb}$ at inhibiting activation of $M2_{tb}$	M-units	0.1457
	$M1_2^{\infty}$	Constant controlling the effectiveness of $M1_{tb}$ at inhibiting proliferation and activation of F_{tb}	M-units	0.0843
	$M2^{\infty}$	Constant controlling the effectiveness of $M2_{tb}$ at inhibiting activation of N_{tb} and $M1_{tb}$	M-units	0.4734
	F^{∞}	Constant controlling the effectiveness of F_{tb} at inhibiting the activation of $M2_{tb}$ and $L2_{tb}$	F-units	0.5314
	$L2_1^{\infty}$	Constant controlling the effectiveness of $L2_{tb}$ at inhibiting the activation of N_{tb}, $M1_{tb}$ and $L1_{tb}$	L-units	0.4738
	$L2_2^{\infty}$	Constant controlling the effectiveness of $L2_{tb}$ at inhibiting collateral damage associated with N_{tb} and $M1_{tb}$	L-units	0.4738
Inhibition (radiation-related)	ω_{dam}	Constant controlling the effectiveness of F_{st}^{d} at inhibiting removal of Dam_{tb} by F_{tb}	F-units	0.02
	ω_{m2}	Constant controlling the effectiveness of $\bar{M}_{st}^{d}$ at inhibiting activation of $\bar{M}_{st}^{ud}$ and $\bar{M}_{st}^{d}$ to $M2_{tb}$	M-units	1000
	ω_f	Constant controlling the effectiveness of F_{st}^{d} at inhibiting proliferation of F_{tb}	F-units	0.02
	γ_n	Constant controlling the effectiveness of $Dose_{rad}$ at inhibiting $\bar{N}_{bv}$ infiltration to the surrounding tissue	Gy/h	0.1667
	γ_m	Constant controlling the effectiveness of $Dose_{rad}$ at inhibiting $\bar{M}_{bv}$ infiltration to the surrounding tissue	Gy/h	0.1

	γ_l	Constant controlling the effectiveness of $Dose_{rad}$ at inhibiting L_{bv} infiltration to the surrounding tissue	Gy/h	0.1667
	γ_f	Constant controlling the effectiveness of $Dose_{rad}$ at inhibiting F_{ct} infiltration to the surrounding tissue	Gy/h	0.05
Damage/Debris	k_{dn}	Maximum collateral tissue damage rate caused by N_{tb} at the local wound site	D-units/h	0.000175
	k_{dm1}	Maximum collateral tissue damage rate caused by $M1_{tb}$ at the local wound site	D-units/h	$\sigma_{dm1} \cdot k_{dn}$
	σ_{dm1}	Tissue damage scaling coefficient for $M1_{tb}$	Unitless	0.5
	N_H	Hill constant for tissue damage associated with N_{tb}	N-units	0.06
	$M1_H$	Hill constant for tissue damage associated with $M1_{tb}$	M-units	0.06
	ρ_{dam}	Baseline tissue damage repair rate via a combination of repair, resolution, and regeneration	1/h	0.004
	k_{df}	Repair rate on Dam_{tb} by F_{tb}	1/(F-units·h)	0.02
	k_{dnp}	Phagocytosis rate of Deb_{tb} by N_{tb}	D-units/(N-units·h)	0.013
	k_{dm1p}	Phagocytosis rate of Deb_{tb} by $M1_{tb}$	D-units/(M-units·h)	0.0176
	k_{dm2p}	Phagocytosis rate of Deb_{tb} by $M2_{tb}$	D-units/(M-units·h)	0.0101
	d_{deb}	Decay rate of Deb_{tb}	1/h	0.0001
Neutrophils	s_{nr}	Recruitment rate of circulating neutrophils $\bar{N}_{bv}$ to the local wound site	N-units/h	0.0137
	d_{nr}	Decay rate of $\bar{N}_{st}^{ud}$	1/h	0.019
	d_n	Decay rate of N_{tb}	1/h	0.0206
	k_{nd}	Activation rate of resting neutrophils $\bar{N}_{st}^{ud}$ to N_{tb} by Deb_{tb}	1/(D-units·h)	0.2432
	k_{np}	Activation rate of resting neutrophils $\bar{N}_{st}^{ud}$ to N_{tb} by P_{tb}	1/(P-units·h)	7.325
	k_{nn}	Activation rate of resting neutrophils $\bar{N}_{st}^{ud}$ to N_{tb} by N_{tb} and its byproducts	1/(N-units·h)	0.0169
	k_{nm1p}	Phagocytosis rate of N_{tb} by $M1_{tb}$	1/(M-units·h)	0.1208
	k_{nm2p}	Phagocytosis rate of N_{tb} by $M2_{tb}$	1/(M-units·h)	0.3628

Macrophages	s_{mr}	Recruitment rate of fixed tissue and circulating monocytes to the local wound site	M-units/h	1.7575
	d_{mr}^{ud}	Decay rate of $\bar{M}_{st}^{ud}$	1/h	0.0221
	d_{mr}^{d}	Decay rate of $\bar{M}_{st}^{d}$	1/h	0.005
	d_{m1}	Decay rate of $M1_{tb}$	1/h	0.0497
	d_{m2}	Decay rate of $M2_{tb}$	1/h	0.1236
	k_{m1d}	Activation rate of resting monocytes $\bar{M}_{st}^{ud}$ and $\bar{M}_{st}^{d}$ to $M1_{tb}$ by Deb_{tb}	1/(D-units·h)	0.0035
	k_{m1p}	Activation rate of resting monocytes $\bar{M}_{st}^{ud}$ and $\bar{M}_{st}^{d}$ to $M1_{tb}$ by P_{tb}	1/(P-units·h)	0.00015433
	k_{m1n}	Activation rate of resting monocytes $\bar{M}_{st}^{ud}$ and $\bar{M}_{st}^{d}$ to $M1_{tb}$ by N_{tb} and its byproducts	1/(N-units·h)	0.0346
	k_{m1m1}	Activation rate of resting monocytes $\bar{M}_{st}^{ud}$ and $\bar{M}_{st}^{d}$ to $M1_{tb}$ by $M1_{tb}$ and its byproducts	1/(M-units·h)	0.000037879
	k_{m1l1}	Activation rate of resting monocytes $\bar{M}_{st}^{ud}$ and $\bar{M}_{st}^{d}$ to $M1_{tb}$ by $L1_{tb}$ and its byproducts	1/(L-units·h)	0.00015542
	k_{m2m1}	Activation rate of resting monocytes $\bar{M}_{st}^{ud}$ and $\bar{M}_{st}^{d}$ to $M2_{tb}$ by $M1_{tb}$ and its byproducts	1/(M-units·h)	0.0219
	k_{m2m2}	Activation rate of resting monocytes $\bar{M}_{st}^{ud}$ and $\bar{M}_{st}^{d}$ to $M2_{tb}$ by $M2_{tb}$ and its byproducts	1/(M-units·h)	0.00067667
	k_{m2l2}	Activation rate of resting monocytes $\bar{M}_{st}^{ud}$ and $\bar{M}_{st}^{d}$ to $M2_{tb}$ by $L2_{tb}$ and its byproducts	1/(L-units·h)	0.0049
	θ_{m1m2}	Transition rate of $M1_{tb}$ to $M2_{tb}$	M-units/N-units	0.6901
Fibroblasts	s_f	Non-injury recruitment rate of fibroblasts to the local wound site	F-units/h	0.0014
	k_{sttb}^{ud}	Rate of transition of undamaged fibroblasts (F_{st}^{ud}) from the surrounding tissue to the thermal burn	1/h	0.0042
	k_{sttb}^{d}	Rate of transition of damaged fibroblasts (F_{st}^{ud}) from the surrounding tissue to the thermal burn	1/h	0.0012
	d_{fr}^{ud}	Decay rate of F_{st}^{ud}	1/h	0.0091
	d_{fr}^{d}	Decay rate of F_{st}^{d}	1/h	0.00090909
	d_f	Decay rate of F_{tb}	1/h	0.0091
	k_f	Baseline proliferation and activation rate of F_{tb}	1/h	0.0053
	α_{m2}	Constant controlling the up-regulation of F_{tb} proliferation and activation by $M2_{tb}$	1/(M-units·h)	0.0455

	α_{dam}	Constant controlling the up-regulation of F_{tb} proliferation and activation by Dam_{tb}	1/(D-units·h)	0.0667
T Lymphocytes	$s_{\ell r}$	Recruitment rate of circulating T lymphocytes to the local wound site	L-units/h	0.0283
	$d_{\ell r}^{ud}$	Decay rate of L_{st}^{ud}	1/h	0.0565
	$d_{\ell r}^{d}$	Decay rate of L_{st}^{d}	1/h	0.0283
	k_{l1}	Induction rate of L_{st}^{ud} and L_{st}^{d} to $L1_{tb}$ by $M1_{tb}$	1/(M-units·h)	0.0431
	k_{l2}	Induction rate of L_{st}^{ud} and L_{st}^{d} to $L2_{tb}$ by $M2_{tb}$	1/(M-units·h)	0.0369
	d_{ℓ}	Decay rate of $L1_{tb}$ and $L2_{tb}$	1/h	0.0594
Pathogen	k_{pg}	Growth rate of P_{tb}	1/h	0.4
	P^{∞}	Carrying capacity of P_{tb}	P-units	13.3333
	k_{pb}	Phagocytosis rate of P_{tb} by the background immune response	1/(B-units·h)	0.6
	s_b	Recruitment rate of circulating background immune cells	B-units/h	0.005
	μ_b	Decay rate of background immune cells	1/h	0.002
	k_{bp}	Phagocytosis rate of cells in the background immune response by P_{tb}	1/(M-units·h)	0.0083
	k_{pn}	Phagocytosis rate of P_{tb} by N_{tb}	N-units/h	1.4596
	k_{pm1}	Phagocytosis rate of P_{tb} by $M1_{tb}$	M-units/h	0.0947
	k_{pm2}	Phagocytosis rate of P_{tb} by $M2_{tb}$	M-units/h	0.0947
Cell Survival	a	Number of non-repairable cell kills per $Dose_{rad}$	1/Gy	-
	b	Number of repairable cell kills per $Dose_{rad}^2$	1/Gy^2	-

Notation:

- Dam_{tb} and Deb_{tb} have the same units - D is used to denote their units.
- N, M, F, L, and P denote the units of neutrophils (N_{st}^{ud}, N_{st}^{d}, and N_{tb}), macrophages ($\bar{M}_{st}^{ud}$, $\bar{M}_{st}^{d}$, $M1_{tb}$, and $M2_{tb}$), fibroblasts (F_{st}^{ud}, F_{st}^{d}, and F_{tb}), T lymphocytes (L_{st}^{ud}, L_{st}^{d}, $L1_{tb}$, and $L2_{tb}$), and pathogen (P_{tb}) respectively.
- B denotes the units for the background immune response, including mast cells and natural killer cells.
- Gy denotes the units for radiation dose (in Gray).
- The cell survival parameters a and b do not have estimated values in the current model iteration.

Appendix B. Abbreviations and Acronyms

a	Non-repairable radiosensitivity parameter of the Linear-Quadratic Model
ARA	Applied Research Associates, Inc.
b	Repairable radiosensitivity parameter of the Linear-Quadratic Model
$Dose_{crit}$	Radiation dose corresponding to an average of one-hit per target
DTRA	Defense Threat Reduction Agency
Gy	Gray, unit of ionizing radiation dose
HENRE	Health Effects from Nuclear and Radiological Environment
LQ	Linear Quadratic (Model)
NUDET	Nuclear Detonation
ODE	Ordinary Differential Equation
$p_{survival}$	Probability of cell survival
TDPM	Time-Dependent Physiological Model